NRSP-2
00-13

DI 155600
Drs. G.H. van der KOLFF
EERSTE MEDEWERKER
BCRS PROGRAMMABUREAU

Impact of remotely sensed sea surface temperatures on a numerical weather prediction model

S. de Haan

DELFIRSCOMMISSIE REMOTE SENSING

BCRS 00-13 MD

Informatiecentrum
Rijkswaterstaat
Meetkundige Dienst

19 DEC 2002

Impact of remotely sensed sea surface temperatures on a numerical weather prediction model

S. de Haan
K.N.M.I.

NRSP-2 report 00-13
NRSP-2 project 1.1/AP-08

ISBN 90 54 11 311 1

July 2000

This report describes a project carried out in the framework of the National Remote Sensing Programme (NRSP-2) under responsibility of the Netherlands Remote Sensing Board (BCRS)

Abstract

Numerical weather prediction (NWP) models can profit from input of accurate satellite measured sea surface temperatures (SST). The project 'SST in HIRLAM' studied the feasibility of incorporating remotely sensed SST into HIRLAM (HIgh Resolution Limited Area Model) the NWP model run operationally at KNMI. The aim of the project is to validate sea surface temperatures measured by the AVHRR (Advanced Very High Resolution Radiometer) and to study the impact of assimilation of AVHRR-SST on the forecast quality of HIRLAM.

AVHRR SST is validated against in-situ ship and buoy observations for a number of time periods, spread over the seasons and for the European area. Due to persistent cloud cover over large areas SST-maps are constructed by compositing AVHRR SST-images over longer periods. Three different types of SST-composites are validated. Furthermore, a statistical algorithm is developed in order to perform quality checks on an SST value at a certain location.

The SST fields are assimilated using synoptic SST measurements and 7-days daily updated composites of AVHRR SST. The error characteristics are derived from a four year data set of AVHRR SST recordings at KNMI. In three different time periods two 12-hour HIRLAM high resolution forecast are made over this region one with conventional SST fields and the other with SST fields originating from the AVHRR measurements.

Impact on 2-meter temperature, pressure, 10-meter wind, dew point temperature and latent and sensible heat fluxes are investigated by comparison with (pseudo) observed values of these parameters.

Assimilation of AVHRR SST results in a better SST field. Users of the current operational AVHRR SST product of KNMI will benefit from this. Moreover, HIRLAM profits from this SST field through direct forcing of the model. Therefore implementation of the assimilation scheme is recommended.

Key words: *Sea Surface Temperatures, NOAA-AVHRR, HIRLAM data assimilation*

Executive Summary

Background

Data from the Advanced Very High Resolution Radiometer (AVHRR) on board the NOAA satellites are obtained by direct readout using KNMI's High Resolution Picture Transmission (HRPT) system. One operational application of these observations is a weekly analysis of sea surface temperature (SST) on the North Sea and North Atlantic. This analysis is based on a cloud cleared composite of AVHRR scans amassed over a week.

NWP models will profit from the assimilation of good quality SST observations through an improved specification of their lower boundary condition over sea and the associated improvement in the modeling of air-sea exchanges. HIRLAM (HIgh Resolution Limited Area Model) is the NWP model run operationally at KNMI. The current surface analysis scheme of HIRLAM uses AVHRR SST observations implicitly through the use of coarse resolution SST analysis maps on 2.5 degree grid prepared by the National Centers for Environmental Prediction, NCEP, part of the NOAA-organization.

Objectives

The objective of this study is to assess the quality of the AVHRR operational product through comparison with independent conventional SST observations. Following this assessment the feasibility of incorporating remotely sensed SST in operational NWP and their impact on forecast quality is studied by assimilation in the operational short range weather forecasting system HIRLAM. This study will support a decision on the operational use of AVHRR SST and SST data obtained from similar instruments on board current and future platforms.

Approach

SST maps for the North Atlantic based on NOAA AVHRR observations are produced at KNMI once a week and are available in digital format for inclusion in NWP models. These digital SST maps form the bases of this study.

The following steps have been taken in conducting this study:

- AVHRR SST observations are validated using conventional SST observations and by comparison with HIRLAM SST analyses. Error statistics for use in data assimilation are derived.

- Impact of AVHRR SST on the forecast quality of HIRLAM is evaluated in a case study in which the HIRLAM SST is replaced by the AVHRR SST.
- The impact of AVHRR SST observations is evaluated by introducing them into the HIRLAM surface analysis scheme, after it has been modified to incorporate this new type of observation.

HIRLAM

The NWP model HIRLAM is used to study the impact. This operational model is used in routine weather forecasting at KNMI. The forecast region is a square which covers a large part of the Atlantic Ocean up to the Caspian Sea. The grid point distance is approximately $50km$.

Validation of AVHRR SST

Throughout summer 1998 and winter 1999 four periods are chosen within which AVHRR SST has been validated using buoy and ship observations. Apart from the operational weekly composite two other composites are generated for validation. The three composites used are:

- 7-day composite, updated once a week (every Monday),
- 7-day composite, updated every day,
- 3-day composite, updated every day,

A complementary cloud clearing algorithm has been developed to remove pixels which are contaminated by low or semi transparent clouds. This algorithm is based on a threshold value for the standard deviation in a close region around the observation location. The 7-day daily updated composite scored best with respect to the RMS of the measured SST and AVHRR SST. This composite had a RMS of around $1K$ in winter and around $1.5K$ during summer and autumn. The increase of this value is due to so called 'hot spots', local heating of the sea surface by the sun. All types composites had a RMS larger than $1K$ due to the composition period and the lack of diurnal change in these composites.

Error Statistics and Assimilation Scheme

Based on a four year data set of weekly composites, correlation functions have been determined for use in the assimilation scheme. Correlation functions describe the spatial coherence between two AVHRR SST observations. These functions are found to depend upon distance, season and geographical position (i.e. North Sea or Atlantic Ocean).

Impact study

An impact study is performed with a $20km$ resolution of HIRLAM. The experiment region was roughly a square from Iceland to Corsica, covering the North Sea with the Netherlands almost in the center. Two types of experiments were performed, one with the conventional SST and the other with assimilated AVHRR SST. Three time periods were selected: summer 1998, spring 1999 and autumn 1999. Through comparison with observed values of temperature at 2 meter, wind at 10 meter, dew point temperature at 2 meter, pressure and pressure reduced to mean sea level the impact of AVHRR SST is quantified. Forecasted 2-meter temperatures during low wind speed observations showed a positive impact, above land and sea. Above land, high wind speed benefited from AVHRR SST. Forecasted sensible heat fluxes were in better agreement with simulated observations of the sensible heat flux when assimilated AVHRR SST was used. Heat fluxes influence a NWP model through direct forcing. The fact that a positive impact on forecasted sensible heat flux does not necessarily imply an improvement in response parameters (i.e wind) is probably caused by the boundary approximation of the model.

Conclusions

Assimilation of AVHRR SST results in a better SST field. All users of the current operational AVHRR SST product of KNMI will benefit from this. Moreover, HIRLAM can profit from this through direct forcing of the model. Investigation and improvement of the boundary layer description of HIRLAM can enlarge the impact of the use of assimilated AVHRR SST. Implementation of AVHRR SST in the assimilation scheme is recommended, keeping in mind that in the near future the coverage in space and time of high quality AVHRR SST observations will increase.

Future

In 2001, AVHRR SST of the whole North Atlantic at $10km$ resolution will be available for the European metereological community through the EUMETSAT 'Ocean and Sea Ice SAF'. These products will be based on existing NOAA-satellites and the new European geostationary satellite MSG (Meteosat Second Generation). The developed assimilation scheme and correlation functions are applicable to these products. In the near future locally received AVHRR SST in Spain and Ireland will be shared within the HIRLAM community. The assimilation scheme and correlation functions are suitable to handle this data.

Preface

The 'SST in HIRLAM'-project has been jointly funded by KNMI and the Netherlands Remote Sensing Board (BCRS). The project (BCRS project no. 1.1/AP-08) started in April 1998 and was carried out at KNMI in De Bilt (the Netherlands).

During this project a paper was presented at the EUMETSAT Meteorological Satellite Data Users' Conference in Copenhagen in September 1999. Subject of this paper was the validation study of AVHRR SST. In May 2000 a paper will be presented at the next EUMETSAT Metereological Satellite Data Users' Conference, held in Bologna. The subject of this paper is the impact study carried out and described in this report.

The author likes to thank Hans Roozekrans of KNMI for his support and discussions on AVHRR SST, for feedback on this report and for writing Appendix D. The author is grateful to Ben Wichers Schreur for getting started with the NWP model HIRLAM, discussions concerning assimilation, verification and impact, and for screening this report.

Contents

Abstract i

Executive Summary iii

Preface vii

1 Introduction 1

1.1 Usage of satellite data in NWP: present state 1

1.2 Objective of this study 3

1.3 Technical approach 3

1.4 Summary of contents 4

2 Background information 5

2.1 HIRLAM 5

2.2 Conventional SST Observations 7

2.3 AVHRR SST observations 8

3 Validation of AVHRR SST 11

3.1 In-situ Observations 11

3.2 AVHRR SST 12

3.3 Validation results 14
3.3.1 AVHRR versus in-situ: June 22 - July 5, 1998 14
3.3.2 AVHRR versus HIRLAM: June 22 - July 5, 1998 . . . 17
3.3.3 All periods 20
3.4 Conclusions 21

4 Assimilation and Error statistics **23**
4.1 Autocorrelation 24
4.2 Approximation of Autocorrelation 25
4.3 Optimal Interpolation 28
4.4 Conclusions 30

5 Impact study **33**
5.1 Experiments 33
5.2 Weather and SST during the experiments 35
5.2.1 June 22 - July 4, 1998 35
5.2.2 May 1 - May 14, 1999 38
5.2.3 September 20 - October 4, 1999 40
5.3 Impact Results 42
5.3.1 Observed pressure 43
5.3.2 Observed pressure reduced to mean sea level 44
5.3.3 Observed 2-meter temperature 45
5.3.4 Observed 2-meter dew point temperature 47
5.3.5 Observed 10-meter wind vector difference 48
5.3.6 Simulated heat flux observations above sea 48

5.4 Summary and Conclusions 51

5.4.1 Summary 51

5.4.2 Conclusions 54

6 Conclusions and remarks **55**

6.1 Outlook 57

A Influence of cold/warm water fronts on S^2 **61**

B Autocorrelation of weekly AVHRR images **65**

B.1 Seasonal autocorrelation 65

B.2 Horizontal distribution of autocorrelation 68

C Impact results **71**

D Validation study of AVHRR SST's in framework of Rest3D project **79**

D.1 Introduction 79

D.2 Objective of study 80

D.3 Working method 81

D.4 Results 81

D.5 Conclusions 84

Chapter 1

Introduction

1.1 Usage of satellite data in NWP: present state

The use of remotely sensed meteorological data as input for numerical weather prediction models (NWP) is not common yet, however the number of types of observations used is increasing. The accuracy of satellite derived observations is known for some types, such as sea surface winds, however there are still problems to tackle in order to incorporate these observations in NWP models. Each type of observation requires a thorough investigation of accuracy and reliability. A large scientific community is researching methods to improve the accuracy of this data source or even to extract other meteorological data from spaceborne measurements.

The (global) coverage, the high temporal and/or spatial resolution of satellite derived observations have proven to be very useful for meteorologists to interpret the state of the atmosphere. Nowadays they frequently use satellite images or derived products for this purpose such as cloud motion animation and water vapor images. These satellite data, conventional observations and the output of NWP models are essential in order to make a reliable weather forecast for more than two or three days ahead.

The very first NWP models were initialized using conventional synoptic observations. The use and improvement of statistical methods to weigh obser-

vations increased the quality of the initialization of the model fields. This initialization is called the analysis of the atmosphere and is performed using a so-called assimilation scheme. The conventional observations have in general a good temporal resolution and, above land, a good spatial resolution. Above sea, however the spatial resolution is poor and therefore remotely sensed observations such as sea surface winds, sea surface temperatures and radiative fluxes can fill this information gap in these regions.

Remotely sensed sea surface wind has proven to be valuable for NWP models. Since several years the European Center for Medium-Range Weather Forecasts (ECMWF) and the United Kingdom Meteorological Office (UKMO) are using sea surface winds derived from the ERS scatterometer. At KNMI these wind observations will soon be used in the analysis scheme of the operational NWP model HIRLAM (High Resolution Limited Area Model).

Another type of observation which is suitable for use in an analysis scheme is satellite derived sea surface temperatures (SSTs). At KNMI SSTs are obtained from the Advanced Very High Resolution Radiometer (AVHRR) on board of the NOAA satellites which are in polar orbit. The spatial resolution can be 1 km with an accuracy of approximately 0.5 K. One operational application of these observations is a weekly analysis of SST on the North Sea and the North Atlantic. This analysis is based on a cloud cleared composite of AVHRR scans amassed over a week. At UKMO a mesoscale AVHRR SST analysis, using daily composites of AVHRR passings, is developed and validated using buoy and ship observations, see [O'Carroll & Candy]. This scheme is not yet used in the regional UKMO-NWP model. At the U.S. National Meteorological Center (NMC) assimilated SSTs are used in the analysis scheme, see [Derber]. The NMC SSTs are updated daily as described by [Reynolds & Smith].

Within the EUMETSAT community projects have started to be prepared for the huge amount of data that will flood the meteorogical community when the Meteosat Second Generation is in operation. Its launch is planned for late 2000 and data will be available for the meteorological community in 2001. In this context the 'Ocean and Sea Ice Satellite Application Facility' will produce AVHRR SST of regions far beyond the range of the KNMI AVHRR receiver. The instrument on this new stationary satellite will be similar to AVHRR. These products will have a spatial resolution of 10 km and will be available in near real time each 3 hours and cover the whole Atlantic Ocean.

The added value of these products to the current KNMI SST product is evident.

NWP models will profit from the assimilation of good quality SST observations through an improved specification of their lower boundary condition over sea and the associated improvement in the modeling of air-sea exchanges. The current surface analysis scheme of HIRLAM uses AVHRR SST observations implicitly through the use of coarse resolution SST analysis maps with a 2.5 degree grid prepared by the National Centers for Environmental Prediction, NCEP (formerly NMC), part of the NOAA-organization.

1.2 Objective of this study

The objective of this study is to assess the quality of the AVHRR operational product through comparison with independent conventional SST observations. Following this assessment the feasibility of incorporating remotely sensed SST in operational NWP and their impact on forecast quality is studied by assimilation in the operational short range weather forecasting system HIRLAM. This study will support a decision on the operational use of AVHRR SST and SST data obtained from similar instruments on board current and future platforms.

1.3 Technical approach

The following steps are investigated in this study

1. AVHRR SST observations are validated using conventional SST observations and by comparison with HIRLAM SST analyses. Error statistics for use in data assimilation are derived.

2. Impact of AVHRR SST on the forecast quality of HIRLAM is evaluated in a case study in which the HIRLAM SST is replaced by the AVHRR SST.

3. The impact of AVHRR SST observations is evaluated by introducing them into the HIRLAM surface analysis scheme, after it has been modified to incorporate this new type of observation.

1.4 Summary of contents

The operational NWP model of KNMI, HIRLAM, is discussed in Chapter 2 together with the operational AVHRR SST product of KNMI and some information concerning the conventional buoy and ship SST observations. In Chapter 3, the validation of AVHRR SST with respect to buoy and ship observations is presented as well as a comparison with HIRLAM SST. Conventional observations are compared to three kinds of composites. Also a statistical algorithm to improve the AVHRR SST is described in this chapter. The error statistics for use in data assimilation are discussed in Chapter 4 together with the data assimilation scheme used in the impact study. Chapter 5 contains the results of the impact study of AVHRR SST in a number of periods. The last chapter contains conclusions and recommendations.

Chapter 2

Background information

In this chapter background information is presented on the NWP model HIRLAM, the framework, the international corporation and usage. The conventional sea surface temperature (SST) observations and AVHRR SST are also discussed here.

2.1 HIRLAM

HIRLAM (High Resolution Limited Area Model) is the operational numerical weather prediction model (NWP) at KNMI and is developed in cooperation with a number of European meteorological institutes. The international HIRLAM project has started in 1985 and is a cooperation of the following meteorological institutes: DMI, DNMI, FMI, IMS, INM, SMHI, VI and KNMI respectively the Danish, Norwegian, Finish, Irish, Spanish, Swedish, Icelandic and Dutch meteorological institute. There is a research cooperation with Météo-France the national meteorological institute of France. The current HIRLAM reference system is used in routine weather forecasting by DMI, FMI, IMS, INM, SMHI and KNMI.

The current operational HIRLAM NWP at KNMI, from now on simply called HIRLAM, runs on a horizontal grid resolution of 164×130 with a grid point distance of $50km$ and a vertical resolution of 31 levels. The region of HIRLAM spans the Atlantic Ocean, the origin of most of our weather, up

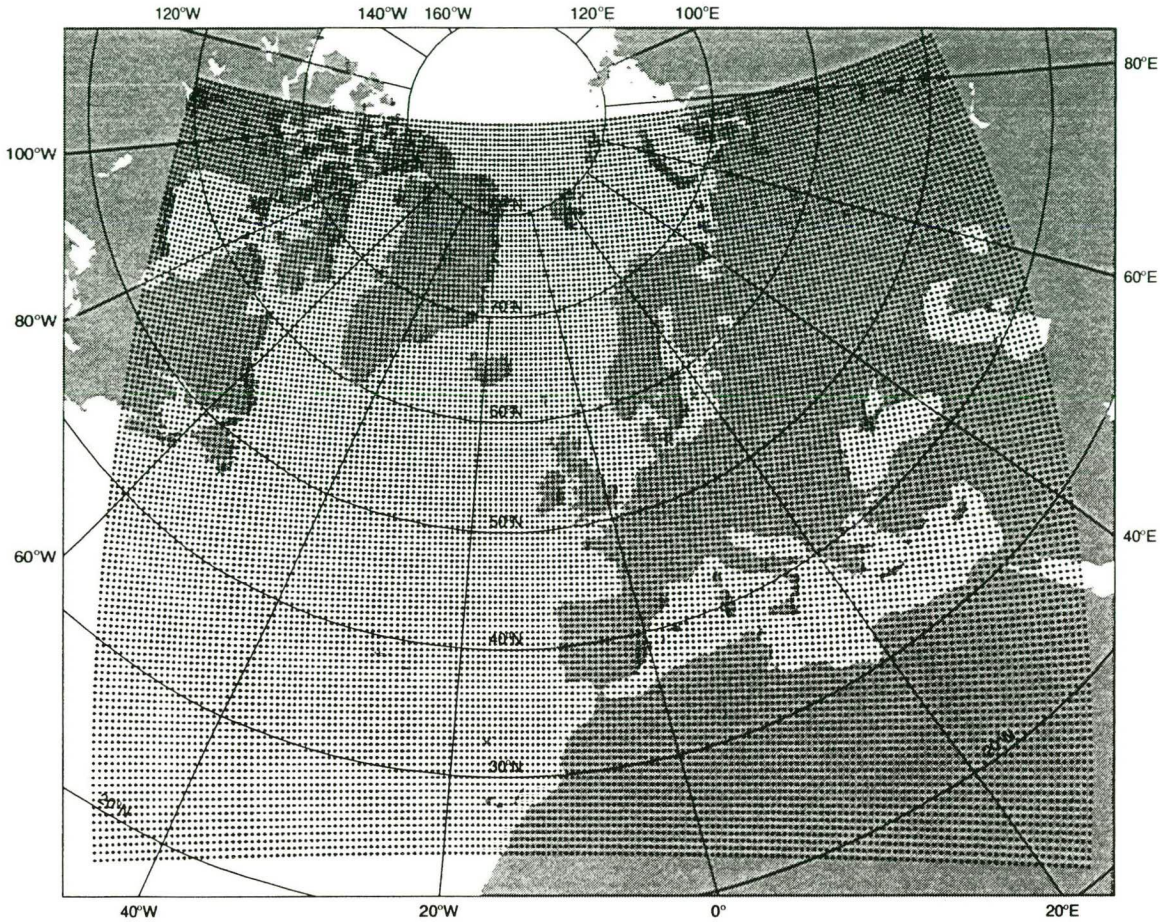

Figure 2.1: Horizontal grid of HIRLAM.

to the Caspian Sea, see Figure 2.1.

HIRLAM is a limited area model which implies that at the boundaries external information is needed for each time step of the forecast. The boundaries used in the operational suite are forecasts of the ECMWF global model, which does not have a boundary problem, however, has a coarser grid.

The initialization of the interior of the model is performed in an analysis step which uses a first guess of the present state of the atmosphere and observations to adjust to a possible best guess. Usually a previous forecast

is taken as the first guess. The whole analysis and initialization process is also called data assimilation. This technique involves a statistical method in order to filter suspicious or wrong observations.

Numerical modelling is the process of obtaining an objective forecast of the future state of the atmosphere by solving a set of equations that describe the evolution of variables (temperature, wind speed, humidity, pressure) that define the state of the atmosphere. All numerical models of the atmosphere are based upon the momentum equations, the thermodynamic and moisture conservation equations, the hydrostatic equation and the continuity equation. Numerical models differ in the approximations and assumptions made in the application of these equations, how they are solved to make a forecast and in the physical parametrizations. The lower atmosphere is approximated different from the upper atmosphere, due to for example surface friction which can cause turbulence.

HIRLAM produces 48 hour forecasts of all important physical parameters such as wind speed and direction, air temperature at 2 meter etc. Because of the high resolution HIRLAM is able to predict small scale weather phenomena better than global models which, due to computational capacity have a much coarser grid. A drawback is the fact that boundary information derived from the coarse global forecasts needs to be present and this information will introduce additional errors at these boundaries. These errors will travel into the region and thus set an upper limit to the forecast length to ensure reliability and representativity of the HIRLAM forecast.

The currently used sea surface temperature (SST) in HIRLAM is assimilated using the coarse SST analysis maps prepared by the National Centers for Environmental Prediction (NCEP), formerly NMC, of NOAA, together with ship and buoy measurements of SST. The NCEP SST map has a grid of 2.5 degrees over the whole globe.

2.2 Conventional SST Observations

Conventional SST observations are performed using a puts, at the water inlet of a ship or with a skin sensor. In almost all cases the reported SST is the bulk SST that is the water temperature at a depth of approximately one me-

ter. The SST measurements are delivered through the normal meteorological communications network called Global Telecommunications System (GTS). The observed SST can be erroneous due to the fact that there can be errors in position, in malfunctioning of the instrument or transmission of the data. Especially automatic (i.e. buoy) observations need a lot of attention.

2.3 AVHRR SST observations

Starting in 1990 for the North Sea and in 1995 for all European seas within the coverage of its HRPT-station KNMI operates a semi-automatically running system for the production of AVHRR SST maps on a routine basis. AVHRR data of all NOAA-passes received by the KNMI antenna are processed in real time. Images are cloud cleared using the APOLLO scheme of Saunders and Kriebel [Saunders & Kriebel]. The SSTs are calculated using the split window coefficients of Llewellyn-Jones et al. [Llewellyn-Jones et al.]. Automatic navigation is performed using daily refreshed TBUS data. All images are polar stereo-graphical projected with a pixel resolution of 2 km. Exact navigation of these images is done manually by coastline fitting using a land/sea mask. Operationally, once a week (every Monday) all images received and processed in the week before are composed into one SST map covering all European waters. For each pixel the maximal occurring SST value is chosen in the weekly composite map. In this way the cloud contaminated pixels are mostly eliminated due to the fact that the temperature of clouds is usually lower than the SST. However, very persistent clouds, which are not unusual in the mid-latitudes, still will be present. See for example the region north-east of Ireland in Figure 2.2b.

At the MetOffice of the United Kingdom an SST product is produced at 1km resolution, see [O'Carroll & Candy]. It covers the North Sea, the Bay of Biscayne and a part of the North Atlantic Ocean. This product is smaller than the KNMI SST product and is based on daily composites. The processing contains a cloud clearing step to select clear sky observations made by the AVHRR instrument and then use a linear combination of measurements from different infra-red window channels to estimate the surface temperature, similar to the procedure used at KNMI.

The radiation observed by AVHRR actually originates from the skin of the

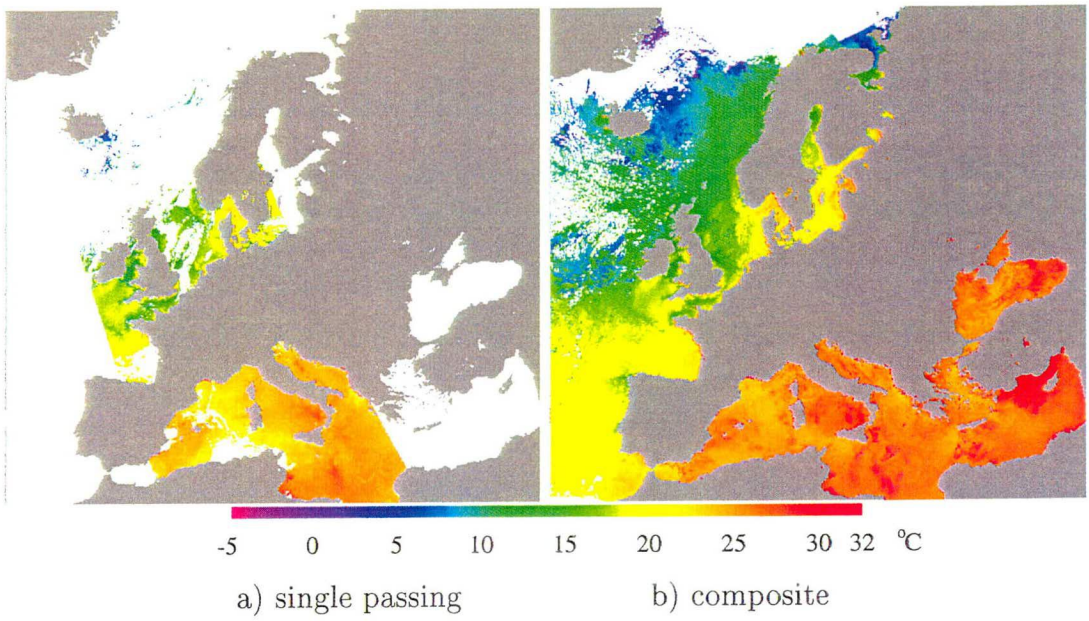

Figure 2.2: SST measured by the NOAA-AVHRR sensor: a) the measured SST for a single passing on 12th July 1999; Figure b) is the composite of images in week 28 in 1999 (12-18 July). White pixels represent clouds or no data; grey pixels land.

ocean. Depending on the direction of the heat flux between the ocean and atmosphere the skin SST can either be cooler or warmer than the underlying bulk SST. These variations usually lie in the range between -1 and +1 K. During the day under dual conditions of high insolation and low wind speed the so-called diurnal thermocline, warm near surface layer can build up which can cause the observed AVHRR SST to be a few degrees warmer than the bulk SST, see [Candy & Anderson] and [Anderson, et al.].

Chapter 3

Validation of AVHRR SST

In this chapter AVHRR SST values are validated using conventional observations. The reported accuracy of conventional observations is discussed in the first section. Cloud contamination, remarks concerning coastal areas and a statistical algorithm to improve the AVHRR SST are presented in the Section 3.2. Section 3.3 contains the actual validation. The last section, Section 3.4, contains conclusions drawn from the validation results.

3.1 In-situ Observations

To validate AVHRR SST a data-set of in-situ observations is required. This data-set is obtained from the Real Time Waarnemings Database (RTWNDB) which is a collection of all observations which arrive at KNMI through the GTS. All observations in the database are stored in a prescribed format with a certain accuracy. The location is reported with a accuracy of one tenth of a degree latitude and longitude. For lower latitudes the location is accurate however for higher latitude, for example regions close to Iceland rounding to tenth of degrees introduces an uncertainty in location of around 7km. The SST is reported also in tenth Kelvin and this is assumed to be accurate enough.

The reports itself in the RTWNDB can be invalid. The observations in the database are not checked with respect to correctness and consistency. The

deviations from the actual SST can originate from malfunctioning of apparatus, human errors or transmission of the data. Using a cleaning algorithm more or less obvious errors are removed from the data-set. This algorithm is described below. The algorithm performs several checks based upon the measured SST and location.

Observations are not used for validation of AVHRR SST when:

- an unrealistic location occurs
- a sudden and unrealistic large change in location occurs;
- an observation is too close to land (or even on land);
- unrealistic SST (not within the range of -5 to 45° C);
- large difference from the moving averaged SST or a too small number of observations.

The remaining data set is then reduced such that each buoy or ship has a maximal frequency of reporting of four times every 24 hours, to obtain observations with comparable reporting frequencies.

Two week periods are used for the validation. The number of in-situ buoy observations in a period is five times the number of in-situ ship observations, however the buoys do not have a large coverage (see Figure 3.1a) compared to ships (see Figure 3.1b).

3.2 AVHRR SST

AVHRR images are obtained by applying an SST-algorithm on raw AVHRR data. An image has a resolution of $2km \times 2km$ and has 2400×2560 pixels. These images can still contain differences with respect to the bulk SST due to non-detected clouds, inaccuracy of location navigation of the image pixels and locally heating of the upper thin layer of the sea, a so-called 'hot spot'. The differences due to hot spots are more or less natural while the other types of differences are not.

It is known from literature that the AVHRR SST overestimates the bulk SST with approximately half a degree. This is of course the case when the pixel is completely cloud free, see [Anderson, et al.] and Appendix D.

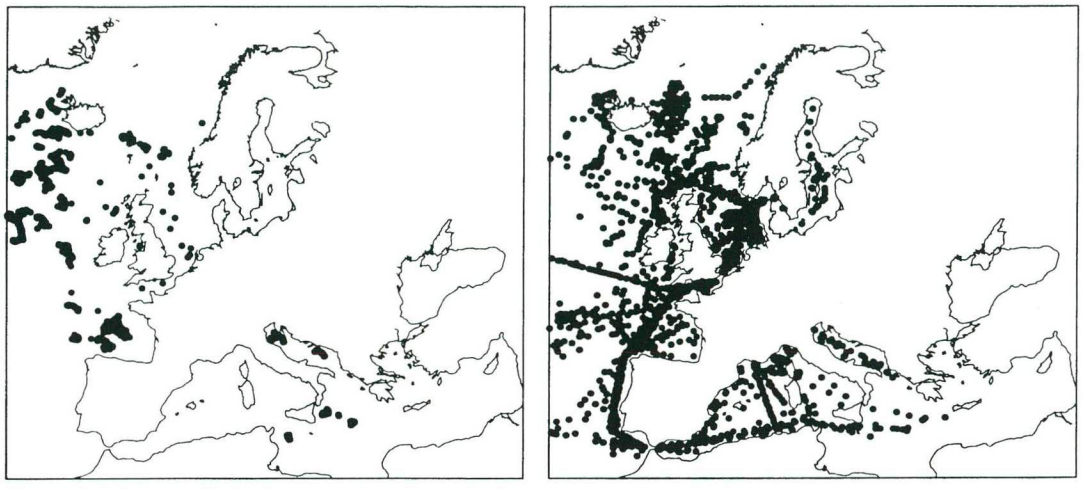

a) Buoy b) Ship

Figure 3.1: Buoy and ship locations between the 22nd of June and the 7th of July.

When a pixel contains a non-detected cloud the bulk SST will normally be underestimated, while a hot spot will result in a overestimation of the bulk SST. The error due to the non-detected clouds can be more or less over-come when a statistical algorithm is used. This algorithm is discussed at the end of this section and in more detail in Appendix A. Inaccuracies of latitude and longitude in the images may be as large as 5 pixels.

The images used below are composites, that is they are the combination of a number of AVHRR images of different times within a certain time period. The pixel value of a composite is the maximum pixel value of the AVHRR images in the specific time period. In the validation the following types of composites are used:

- The current operational SST product which is a composite of AVHRR SST over one week from Monday to Sunday. This composite is abbreviated as 7D-w.
- A composite of AVHRR SST of the past seven days constructed each day. This type of composite is called 7D-d.
- A composite of AVHRR SST of the past three days constructed each day. This type of composite is called 3D-d.

The estimation of the AVHRR SST in a certain position is based on a statistical algorithm. Suppose that an area in a neighborhood (a square of M pixels) of the position under consideration contains N SST-values, T_i, $i = 1..N$ and thus $M - N$ cloud pixels. The sample standard deviation of these N values is:

$$S^2 = \frac{1}{N-1}\sum_{i=1}^{N}(T_i - \bar{T})^2 \tag{3.1}$$

This standard deviation gives information about the distribution of the N SST-values. A large S^2 means a large spread of the SST-value, possibly due to non-detected clouds. The standard deviation is therefore used to distinguish SST-values originating from clear areas and cloudy areas. This is done using a threshold standard deviation S^2_{TH}: data samples with a standard deviation larger than this value will be omitted, while a smaller value will be marked as good.

The threshold value is of major importance. A too small value will result in overestimation of the number of erroneous AVHRR SST, while a too large value will result in a underestimation of the number of erroneous AVHRR SST. Furthermore the threshold value should leave cold/warm water fronts and hot spots intact. Using a threshold value $S^2_{TH} = 2.0$ slow fronts with a temperature difference of $\approx 5K$ and steep fronts with a temperature difference of $\approx 3K$ are recognized. See Appendix A for more details.

3.3 Validation results

In this section the validation results are presented. The bias and root mean square (RMS) are used for the evaluation of the validation. The first period is discussed extensively, the others briefly.

3.3.1 AVHRR versus in-situ: June 22 - July 5, 1998

Below the comparison of the AVHRR SST with in-situ SST in the period from June 22 to July 5, 1998 is presented. The cloud coverage in this period was: Mediterranean Sea cloud free; North Atlantic Ocean 75% coverage;

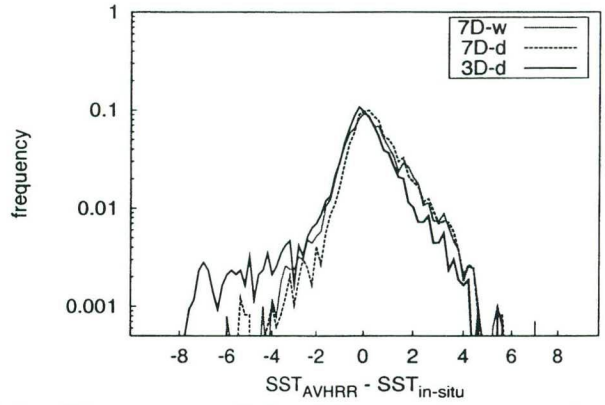

Figure 3.2: Histograms of the difference between the AVHRR SST and the in-situ SST in the period from 22-6-1998 to 5-7-1998. On the horizontal axis is the difference between the AVHRR SST and the in-situ SST, on the vertical axis with a logarithmic scale the percentage of the difference in SST is plotted. All histogram-plots shown here use this scale. A logarithmic scale for the percentage is used in order to emphasize the low percentages.

North Sea, apart from a few days, almost completely covered; Baltic Sea 50% coverage.

In Figure 3.2 the histograms of the difference between the AVHRR SST derived from a composite and the observed in-situ SSTs are shown. In Table 3.1 the percentages of the difference between the AVHRR SST and the in-situ SST are shown. The percentages are accumulated in five intervals: a difference lower than $3K$, between $-3K$ and $-1K$, between $-1K$ and $1K$, between $1K$ and $3K$, and larger than $3K$.

		percentage of $T^{AVHRR} - T^{is}$						
composite	**N**	**< -3**	**-2**	**0**	**2**	**> 3**	bias	RMS
7D-w	5004	1.4	7.1	64.8	22.4	4.3	0.33	1.41
7D-d	4872	1.1	4.2	65.8	24.6	4.3	0.48	1.37
3D-d	4272	5.5	8.3	68.3	15.4	2.5	-0.14	1.67

Table 3.1: The percentages, bias and RMS of the difference between the AVHRR- and the in-situ SST accumulated in five intervals in the first period.

Composites which consist of seven days hardly have large underestimations while three-day composite have some large underestimations, due to the number of days that are nudged in the composite and the fact that the AVHRR SST is the maximum of AVHRR SSTs over the period of composition. The percentages of overestimation for the weekly and the seven-day daily composites are comparable, while the three-day daily has less overestimations. The bias and RMS are also shown in Table 3.1.

The bias of the 3D-d is negative due to a tendency of underestimating caused by persistent semi transparent clouds. The RMS of the 7D-d is the smallest of all, while the 3D-d has the largest RMS. This is most likely due to the presence of small/transparent clouds which are present in the 3D-d composite and are maximized out in the other composites.

The histogram and tables discussed so far are for the whole European region within this period. In Figure 3.3 the histograms of the difference between the in-situ SST and the AVHRR SST respectively for the Mediterranean Sea, the North Sea, the North Atlantic Ocean and the Baltic Sea are shown, as well as the borders of the four regions. In Table 3.2 the percentages of the difference between the AVHRR SST and the in-situ SST are shown.

			percentage of $T^{AVHRR} - T^{is}$				
region	**comp.**	**N**	**< -3**	**-2**	**0**	**2**	**> 3**
Atl. Ocean	7D-w	2871	0.7	5.7	69.0	20.8	3.8
	7D-d	2746	0.7	3.3	71.5	22.1	2.4
	3D-d	2298	5.2	6.6	74.2	13.4	0.7
North Sea	7D-w	1519	2.2	4.7	65.5	24.2	3.3
	7D-d	1515	1.8	4.2	65.0	23.7	5.3
	3D-d	1362	7.6	7.3	67.0	14.4	3.7
Baltic Sea	7D-w	60	5.0	33.3	41.7	20.0	0.0
	7D-d	60	0.0	15.0	61.7	21.7	1.7
	3D-d	60	0.0	28.3	53.3	16.7	1.7
Med. Sea	7D-w	554	2.5	18.1	44.2	25.6	9.6
	7D-d	551	0.7	7.6	40.3	39.6	11.8
	3D-d	552	2.0	15.9	48.5	26.1	7.4

Table 3.2: Table of the percentage of the difference between the AVHRR SST and the in-situ SST for the different regions in the period from 22-6-1998 to 5-7-1998.

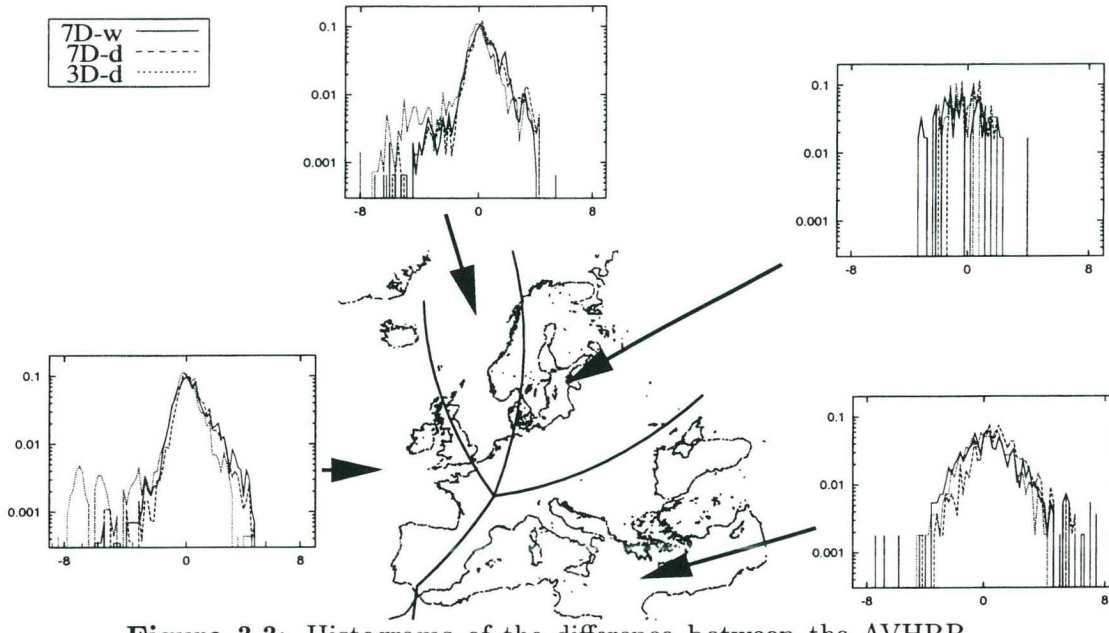

Figure 3.3: Histograms of the difference between the AVHRR SST and the in-situ SST for the Mediterranean Sea, the North Sea, the Baltic Sea and the North Atlantic Ocean in the first period

Large overestimations occur in the Mediterranean Sea most likely due to hot spots. The 7D-d composite has the largest number of overestimations. The North Atlantic Ocean and the North Sea show some overestimations independently of the type of composite used, although less for the three-day daily . See Figure 3.3 and Table 3.2.

Underestimations of the AVHRR SST occur in a large number in the North Sea for all three composites, in the North Atlantic Ocean for the 3D-d-composite, and in the Mediterranean Sea for the 7D-w- and the 3D-d composite. The underestimation in the first two regions is caused by persistent clouds; in the Mediterranean Sea fewer persistent clouds occur.

3.3.2 AVHRR versus HIRLAM: June 22 - July 5, 1998

The AVHRR SST is also compared to the assimilated HIRLAM SST. As said before, the latter SST is assimilated using very coarse AVHRR SST and

in-situ buoy SST. The in-situ measurements used for validation contain buoy as well as ship SST measurements.

SST from the three composites and from the HIRLAM SST field are determined at in-situ locations. AVHRR SST is obtained using the algorithm described in Section 3.2. The HIRLAM SST at the in-situ location is calculated using bi-linear interpolation of the closest four grid point SSTs.

In Figure 3.4(a-c) RMS's of three differences in types of SST are plotted: difference between AVHRR SST and in-situ SST, AVHRR SST and HIRLAM SST and HIRLAM SST and in-situ SST. From this figure it can be seen that overall the RMS of the difference between HIRLAM SST and in-situ is the lowest of all three RMS differences. Furthermore the RMS of the difference between AVHRR SST and in-situ SST is the largest of all three RMS's. This is the case for all three types of composites. The 7D-w and the 7D-d composite have a similar behavior with respect to the RMS's of the

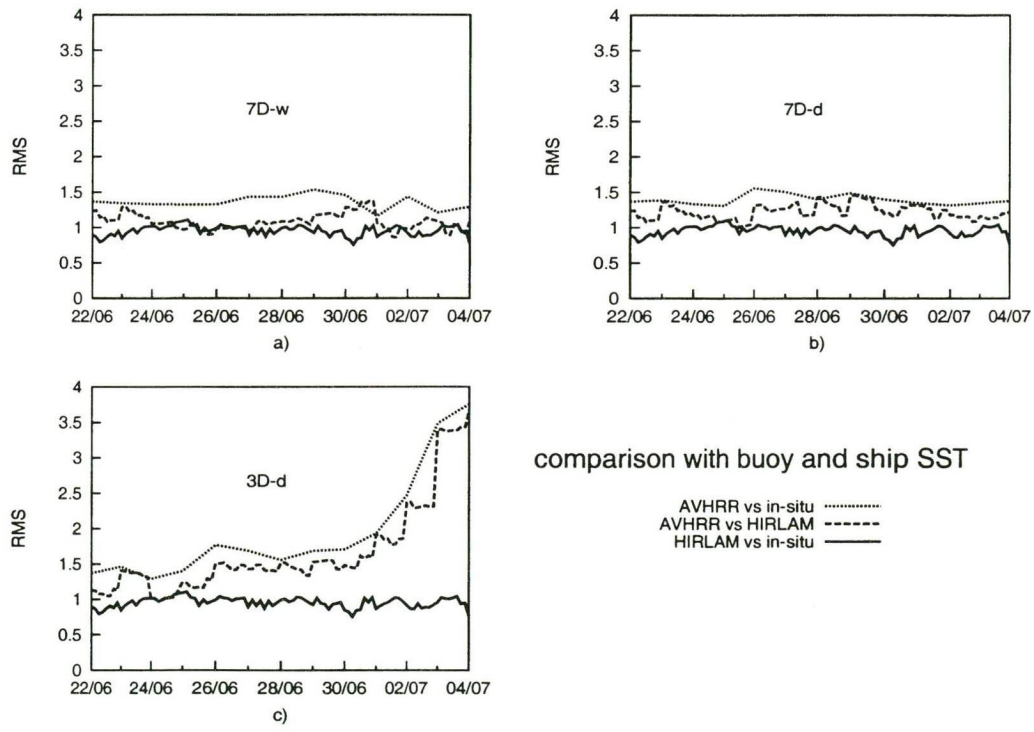

Figure 3.4: RMS's of differences between AVHRR and in-situ SST, HIRLAM and AVHRR SST and HIRLAM and in-situ SST. In-situ SST originates from buoy and ship measurements.

differences, however the 3D-d exhibits an increase in RMS in the first days of July 1998. This is due to one AVHRR passing over the North Sea with reported SST values which are cloud contaminated by low or semi transparent clouds. These SST values passed the cloud filter and the previously discussed statistical algorithm. These low values are not appearing in the 7D-d or 7D-w composites because there were other AVHRR observations in the North Sea with higher SST values in the composite period.

Figure 3.5 is similar to Figure 3.4, however in this figure only in-situ buoy SST are used in the validation. Note that all RMS's are lower. Furthermore the three RMS's obtained using the 7D-d composites are comparable with each other from the 26th of June. This resemblance occurs later in the period when the 7D-w composite is concerned, due to the fact this composite has a more static SST. The 3D-d composite has comparable RMS's for all three types of differences in the first part of this period however increases rapidly

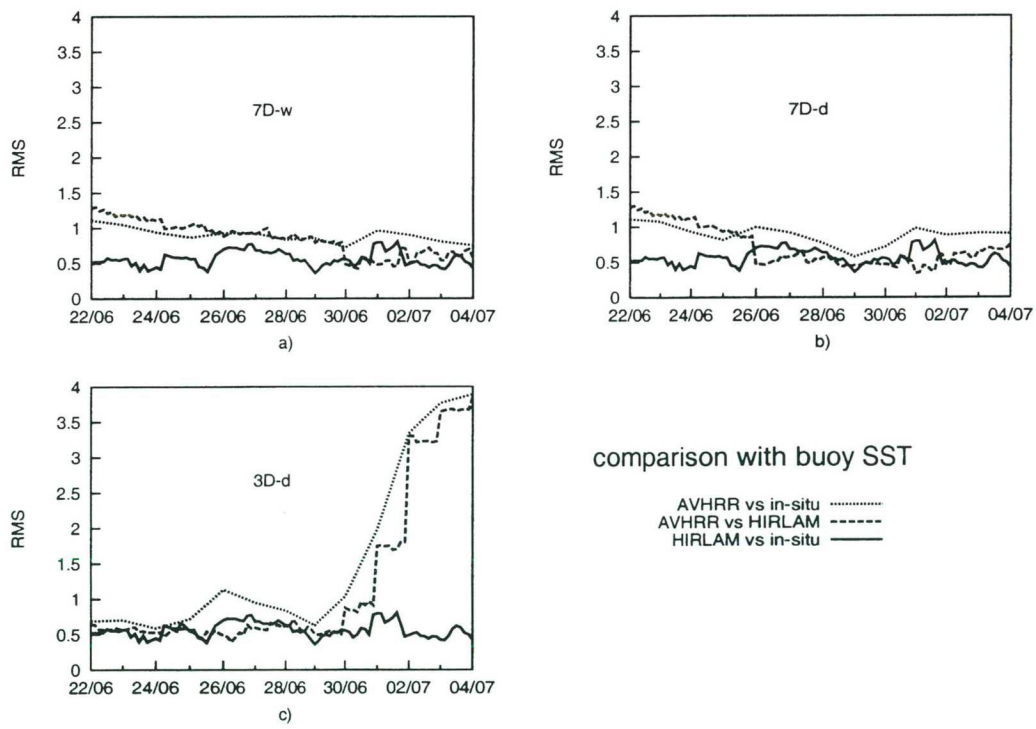

Figure 3.5: RMS's of differences between AVHRR and in-situ SST, HIRLAM and AVHRR SST and HIRLAM and in-situ SST. In-situ SST originates only from buoy measurements.

in the first days of July as explained before.

Note that the RMS of the difference between HIRLAM SST and in-situ SST is now around 0.5K. Assimilation of an in-situ measurement adjusts the SST locally to the observed SST and this effect diminishes with increasing distance to the observation location. In the assimilation scheme a value of the observations error is needed. This value is set to 0.5K in the current HIRLAM SST assimilation scheme, resulting in the shown RMS. For more details on data assimilation see next chapter, Chapter 4.

It seems that AVHRR SSTs are worse than HIRLAM SSTs. This is due to the fact that low or semi-transparent clouds degrade the AVHRR SST. Another problem is, when comparing to in-situ observations that so-called hot-spots are typically a skin phenomenon, and therefore will not be measured by an in-situ observation which measures the bulk SST. This will increase the RMS between AVHRR SST and the in-situ SST and also the RMS between AVHRR SST and HIRLAM SST because in-situ SST information is incorporated in the HIRLAM SST.

3.3.3 All periods

In Table 3.3 the bias and RMS are shown for all examined periods and the three different types of composites.

The 3D-d composite has the smallest bias (except for the fourth period in February), and the 7D-w has the largest bias (again except for February). The biases of all three composites show the same trend in the first three periods: low in June, higher in September and moderate in November.

	bias			**RMS**		
period	**7D-w**	**7D-d**	**3D-d**	**7D-w**	**7D-d**	**3D-d**
22/6/98 - 5/7/98	0.33	0.48	-0.14	1.41	1.37	1.67
6/9/98 - 19/9/98	0.90	0.65	0.24	1.80	1.58	1.46
23/11/98 - 6/12/98	0.52	0.38	-0.28	1.15	1.03	1.98
8/2/99 - 21/2/99	-0.09	-0.05	-1.03	1.83	0.99	2.99

Table 3.3: The bias and RMS for all periods.

The 7D-d composites has the lowest RMS of all three composites in all periods, except for September. The highest RMS occurs for the 3D-d composite (again not for September). The RMS has no clear trend.

3.4 Conclusions

For four periods the AVHRR SST is validated against in-situ SST. This in-situ SST probably still has a diurnal cycle. Therefore, the RMS of the difference between the in-situ SST and a composite over a three or seven day period cannot be (close to) zero.

The period over which the composite is made is of major importance. When the composite period is too small a large number of underestimations will appear possible due to a large number of cloud contaminated pixels. On the other hand a too large period will overestimate the AVHRR SST because the dynamic behavior is less, due to the fact that the maximum AVHRR SST value is used over the whole composite period.

The AVHRR SST originating from a daily updated seven-day composite is generally better than originating from a weekly or three-day daily composite; the RMS is minimal for the seven-day daily composite.

Comparing AVHRR SST with HIRLAM SST results in RMS's of the same order as when HIRLAM SST is compared to in-situ buoy observations.

The advantage of composites is the large area of coverage and more complete coverage. A more recent AVHRR SST validation study, carried out in the framework of the Rest3D project of the BCRS, showed that generally, a single passing has better RMS's ($0.6K$), see Appendix D. However the small and incomplete area that is covered reduces the use as input for NWP models. NWP models need fully prescribed SST fields. Furthermore, by applying a statistical algorithm on the currently created AVHRR SST composites the possibility of using a invalid (i.e. cloud contaminated) SST value is ommited.

With the forthcoming SST products from the Ocean&Sea Ice SAF, the region of coverage can be enlarged to nearly the whole HIRLAM area. Also the quality of the SAF-SST product will be high due to the state-of-the-art processing and validation techniques, see [Anderson, et al.] and [O&SI].

Furthermore, as a first step, there are advanced plans to share locally received AVHRR SST in Spain and Ireland. These SSTs are comparable to the AVHRR SST received at KNMI, and therefore will have an added value.

Chapter 4

Assimilation and Error statistics

Data assimilation is a commonly used technique in NWP for weighting observations to construct a two or three dimensional field of an observed physical parameter. Variational optimalisation, successive corrections and optimal interpolation are frequently used techniques. The first technique minimizes a cost function of the differences between observation and a first guess field. This assimilation technique has benefits for highly dynamical physical parameters especially when it is used in combination with a NWP model. Successive corrections is a recursive algorithm to minimize the difference between a background field and observations. This is a simple technique however it has limitations with respect to the number of observations of a physical parameter. Furthermore all observations whether the origin is in-situ or spaceborne are treated with equal weights without taking into account the number of measurements of each type. Optimal interpolation uses weights based on known horizontal (auto)correlations of a background field, for example climatology. The latter assimilation technique, optimal interpolation, is used here because this technique can handle large amounts of observations and with a natural balance between in-situ and spaceborne SST.

In the next section the definition of (auto)correlation is given. In Section 4.2 the implemented correlation functions are presented which are used in optimalisation scheme. Hereafter, in Section 4.3, the optimal interpolation algorithm for assimilation of AVHRR SST is explained. The last section of this

chapter contains conclusions and remarks concerning (near) future AVHRR SST products.

4.1 Autocorrelation

Autocorrelation is the correlation between two data sets of the same physical property. The data sets should have the same temporal distribution. The physical property here is AVHRR SST; the data set consists of AVHRR SST obtained from weekly composites over a period of four years. In this section a general definition of (auto)correlation is given together with the technique to determine the (auto)correlation using a data set.

The correlation ρ_{XY} of random variables X and Y is defined as

$$\rho_{XY} = \frac{E\{(X - \mu_X)(Y - \mu_Y)\}}{\sigma_X \sigma_Y}, \tag{4.1}$$

where $\mu_X = E(X)$ is the expected value of X also called the mean of X. If for some reason the random variable X is larger than its mean and the same yields for the random variable Y the product $(X - \mu_X)(Y - \mu_Y)$ will tend to be positive. The same will be true if both variables tend to be smaller than their means simultaneously. The correlation is then positive. A negative correlation implies that the variables tend to move in opposite directions with respect to their means. The correlation ρ_{XY} has a range between -1 and +1. When the correlation is ± 1 the random variables are linearly related.

As said before, autocorrelation is the correlation of two data sets with the same physical property. The origin of the difference between the two data sets lies in the location of measurement. Assume the data set $\mathcal{X}$ respectively $\mathcal{Y}$ contains all AVHRR SST weekly composite measurements of the past four yours at location i respectively j, that is

$$\mathcal{X} = \{T_\ell^i : \text{AVHRR SST in } i \text{ in week } \ell\},$$
$$\mathcal{Y} = \{T_\ell^j : \text{AVHRR SST in } j \text{ in week } \ell\}.$$

Let $\mathcal{L}$ be the set containing indices of these two sets for which both $\mathcal{X}$ and $\mathcal{Y}$ have an AVHRR SST. Thus $\mathcal{L}$ contains in time collocated SST indices for these two locations, or

$$\mathcal{L} = \{\ell : T_\ell^i \in \mathcal{X} \text{ and } T_\ell^j \in \mathcal{Y}\}$$

The correlation between locations i and j is then defined as

$$\rho_{ij} = \frac{\sum_{\ell \in \mathcal{L}} \left(T_\ell^i - \bar{T}_\mathcal{L}^i\right)\left(T_\ell^j - \bar{T}_\mathcal{L}^j\right)}{\sqrt{\sum_{\ell \in \mathcal{L}} \left(T_\ell^i - \bar{T}_\mathcal{L}^i\right)^2 \left(T_\ell^j - \bar{T}_\mathcal{L}^j\right)^2}}, \tag{4.2}$$

with,

$$\bar{T}_\mathcal{L}^k = \frac{1}{\#\mathcal{L}} \sum_{\ell \in \mathcal{L}} T_\ell^k \text{ for } k = i, j \tag{4.3}$$

the mean of the collocated SST-values in location i and j of the time series in SST.

The autocorrelation is examined thoroughly in Appendix B for ρ depending on the distance between two points, the latitude of location i and the distance and the season. All these quantities influence the value of the correlation. See Appendix B for more details.

The autocorrelation is defined as a mean of the ρ_{ij} for which i and j satisfy certain criteria (criteria with respect to distance, time or both). For example when the autocorrelation with respect to the distance between two points is examined the autocorrelation is equal to

$$\rho(r) = \frac{1}{\#\mathcal{K}} \sum_{i,j \in \mathcal{K}} \rho_{ij}, \tag{4.4}$$

where the set $\mathcal{K}$ contains all pairs of points for which the distance is between $r - \frac{1}{2}\delta r$ and $r + \frac{1}{2}\delta r$ or,

$$\mathcal{K} = \left\{(i,j) \,:\, r - \frac{1}{2}\delta r \leq \|\mathbf{r}_i - \mathbf{r}_j\| < r + \frac{1}{2}\delta r\right\} \tag{4.5}$$

with $\mathbf{r}_i$ is the location of point i and δr is the so-called bin length. The other definitions are constructed similarly. $\rho(r)$ is also called a structure function.

4.2 Approximation of Autocorrelation

Below the approximation of autocorrelation is presented for weekly AVHRR images from August 1995 up to July 1999. Autocorrelation or structure

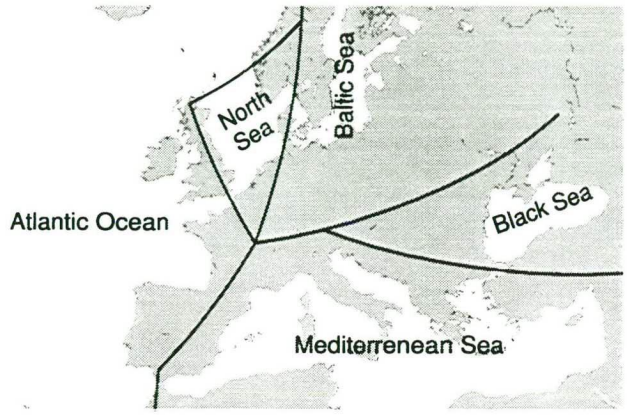

Figure 4.1: The five different seas

functions can be different for different regions and/or seas. An inland sea will have a different correlation structure than the Atlantic Ocean. The seasonal effect can also influence the structure functions. The structure functions are therefore determined for the following regions: Atlantic Ocean, Baltic Sea, Black Sea, North Sea and the Mediterranean Sea, see Figure 4.1.

Based on the numbers calculated and shown in Appendix B a model of the autocorrelation is constructed. The following assumptions are made

- the horizontal structure of the correlation function is rotational symmetric and has an exponentially decay,
- seasons play an important role,
- an additional dependence on the latitude is assumed for the Atlantic Ocean,
- distances larger than 500km for the North Sea, the Baltic Sea and the Black Sea are neglected,
- distances larger than 1000km for the Mediterranean Sea and the Atlantic Ocean are neglected.

See Appendix B for a foundation of these assumptions. The corresponding autocorrelation for the North Sea, the Black Sea, the Baltic Sea and the

Mediterranean Sea is thus approximated by

$$\hat{\rho}(r,\tau) = e^{-r(a_0+a_1\cos(\tau-a_2))^{-1}} \tag{4.6}$$

and for the Atlantic Ocean,

$$\hat{\rho}(r,\tau,\phi) = e^{-r(a_0(\phi)+a_1(\phi)\cos(\tau-a_2(\phi)))^{-1}} \tag{4.7}$$

where ϕ is the latitude and τ represents seasons: $\tau = 0$ stands for spring, $\tau = 0.5\pi$ summer, etc. When a_1 equals zero no seasonal dependence is suspected. The factor $a_0 + a_1\cos(\tau - a_2)$ is the so-called characteristic length scale of the autocorrelation and should be positive. This implies a condition for a_0 and a_1:

$$a_0 - |a_1| > 0.$$

A small characteristic length scale corresponds to correlations of only close AVHRR SST observations. Note that the autocorrelation is positive and has a zero limit for large distances, independent of season and/or latitude. The correlations are determined in bins of 50km.

In Appendix B correlations are shown for the five regions and four seasons. The Levenberg-Marquardt method is used to fit the data of a certain region by $\hat{\rho}$, see [Numerical Recipes] Chapter 14. This method reduces the value χ^2 between $\hat{\rho}$ and the data set by adjusting the coefficients a_0, a_1 and a_2 using a least squares fit. Known standard deviations are also used in the minimization algorithm. Table 4.1 shows the coefficients of $\hat{\rho}$ of the regions without latitude dependence.

The coefficients for the autocorrelation in the Atlantic Ocean for different latitude bands are shown in Table 4.2. The coefficients for the North Sea and

	coefficients of $\hat{\rho}$			$\rho - \hat{\rho}$	
region	a_0 (10^3km)	a_1 (10^3km)	a_2 (rad)	**bias**	**RMS**
Black Sea	2.5	1.1	1.5	-0.05	0.11
Baltic Sea	1.8	1.3	1.6	-0.05	0.10
North Sea	1.2	0.7	1.6	-0.02	0.06
Mediterranean Sea	3.7	2.5	1.9	-0.07	0.13

Table 4.1: Coefficients of $\hat{\rho}$ for four regions. The RMS and bias of the difference between the observed mean autocorrelations and $\hat{\rho}$ with these coefficients.

Atlantic Ocean	coefficients of $\hat{\rho}$			$\rho - \hat{\rho}$	
latitudes (ϕ)	a_0 (10^3km)	a_1 (10^3km)	a_2 (rad)	**bias**	**RMS**
$30^0 - 80^0$	0.6	0.3	2.2	-0.03	0.14
$40^0 - 50^0$	1.1	0.6	2.2	-0.03	0.11
$60^0 - 70^0$	0.4	0.2	2.4	0.01	0.16

Table 4.2: Coefficients of $\hat{\rho}$ for the Atlantic Ocean for different latitudes.The RMS and bias of the difference between the observed mean autocorrelations and $\hat{\rho}$ with these coefficients.

the Atlantic Ocean with the latitude between 40^0 and 50^0 are comparable, see Tables 4.1 and 4.2. The autocorrelation in the North Sea is similar to that of the Atlantic Ocean, with a slight shift in time (coefficient a_2).

The latitude dependence of coefficients of $\hat{\rho}$ approximated by setting

$$a_0(\phi) = 1.4 - 0.015\,\phi,$$
$$a_1(\phi) = 1.2 - 0.015\,\phi,$$
$$a_2(\phi) = 2.2,$$

with ϕ between 30 and 80 degrees.

At the U.S. National Meteorological Center error statistics were derived for their operational global SST analysis. This analyses uses 7 days of in-situ (ship and buoy) and AVHRR SST and are produced on a 1° grid. The average e-folding spatial error scales are found to be $850km$ in the zonal direction and $615km$ in the meridional direction, see [Reynolds & Smith]. No distinction is made with respect to latitude, season or geographical location of the sea. The average of these values are comparable to the values in Table 4.2 when no distinction in latitudes is made.

4.3 Optimal Interpolation

Optimal interpolation is a widely used technique to analyze meteorological data and correspondingly construct meteorological fields. In this section the (formal) definition of optimal interpolation is given and the data flow scheme of this technique is shown. A more complete discussion on this data assimilation technique can be found in [Daley].

Optimal interpolation assumes uncorrelated observation errors and homogeneous background errors. The meteorological data used here are composites from two different NOAA satellites. A correlated observation error can be the case here, although due to the occurrence of semi transparent clouds and the fact that a period of 7 days is used for the composite the correlation of the observation error may be weak. Optimal interpolation is used here to obtain a better coverage of the AVHRR SST field without losing high quality nor adding doubtful information.

Let $\mathbf{r}_0$ be the location of the analysis and $\mathbf{r}_k$, $1 \leq k \leq K$ denote the positions of the observations. The expected background error variance is denoted as E_B^2 and the expected observation error as E_0^2. Define for each observation a posteriori weight W_k. Let T_O, T_B and T_A denote the observed, background and analyzed sea surface temperatures respectively. The background error correlation between two positions i and j is denoted as

$$\rho_{ij} = \rho(\|\mathbf{r}_i - \mathbf{r}_j\|)$$

except for the Atlantic Ocean where

$$\rho_{ij} = \rho(\|\mathbf{r}_i - \mathbf{r}_j\|, \phi_i).$$

The optimal interpolation algorithm is

$$T_A(\mathbf{r}_0) = T_B(\mathbf{r}_0) + \sum_{k=1}^{K} W_k \left(T_O(\mathbf{r}_k) - T_B(\mathbf{r}_k)\right), \tag{4.8}$$

with the weights W_ℓ satisfying:

$$\sum_{\ell=1}^{K} W_\ell \left(\rho_{k\ell} + \frac{E_O^2}{E_B^2}\right) = \rho_{k0}, \ 1 \leq k \leq K \tag{4.9}$$

Each location $\mathbf{r}_0$ is analyzed once using K neighboring observations. For each observation a $K \times K$-matrix is inverted. The computation time increases rapidly with increasing K. Therefore K cannot be chosen too large, while too small values of K diminish the quality of the algorithm.

For each weekly composite this algorithm is applied to obtain an analyzed SST-field. The background used here is the analyzed SST field of the previous day.

The scheme used to assimilate composites of AVHRR SSTs is shown in Figure 4.2. The AVHRR SST are amassed over the previous 7 days. A new assimilated SST is constructed using optimal interpolation and the assimilated SST of the previous day as background. This scheme is recursive and only needs for the very first step a good guess of the background, for which a climatology field is used. Furthermore because the composites are constructed on a daily basis this scheme is operated daily. Buoy and ship

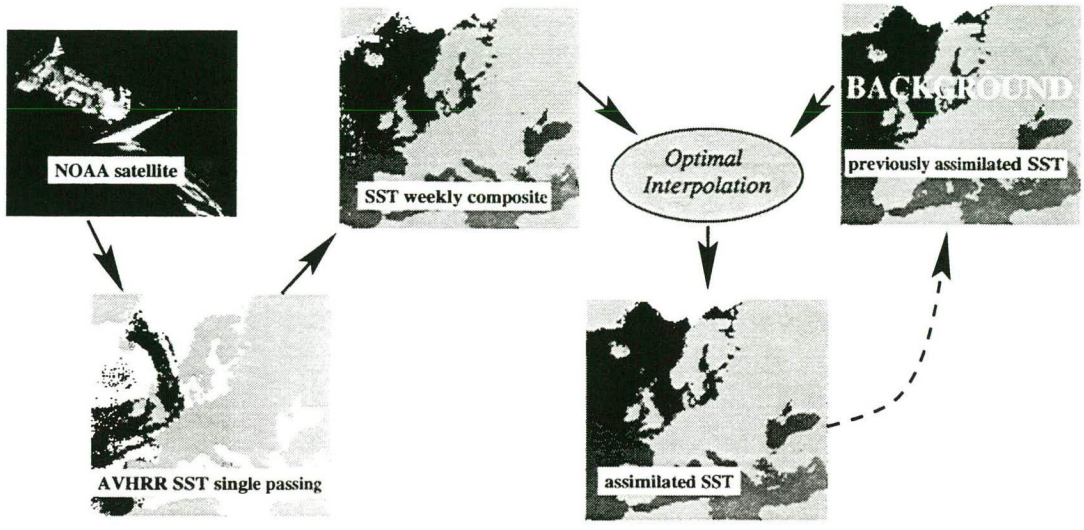

Figure 4.2: Assimilation of AVHRR SST; performed daily.

measurements are used to construct a HIRLAM SST field, see Figure 4.3. These in-situ measurements are exactly the same as those used for the operational HIRLAM SST. The background used for this assimilation step is the assimilated SST of the daily scheme. This scheme can be run at any time of the day, but most preferrably every three hours. Additional to in-situ SST other SST measurements can be added such as AVHRR SST from other satellites.

4.4 Conclusions

In this chapter error statistics were derived for AVHRR SST observations based on a four year data set of weekly composites. Correlations in this data

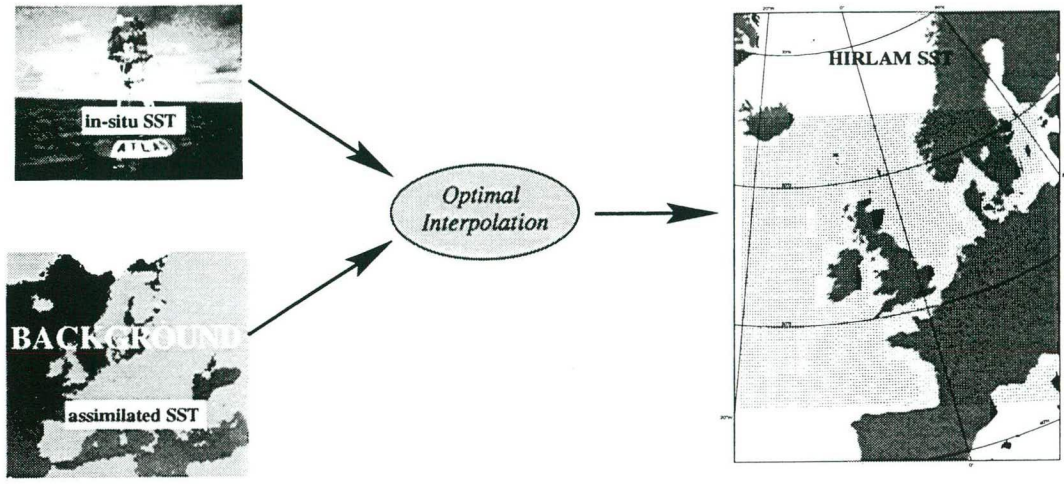

Figure 4.3: Assimilation of in-situ SST; performed each 3 hours.

set are used to fit correlation functions. Correlations between two locations are found to be dependent on distance, time in days and the geographical location of the sea. Correlation functions form the core of the assimilation scheme which is based on the optimal interpolation technique. Using this scheme AVHRR SSTs are prepared for use in HIRLAM.

The assimilation scheme described in this chapter is, with some adjustments applicable to the forthcoming Ocean & Sea Ice SAF SST product. The large coverage (the whole North Atlantic Ocean), high quality (RMS $\approx 0.5K$) and high resolution ($10km$) will have a strong added value to the current operational AVHRR SST product. In 2002 these products will be operationally available for the European meteorological society.

In the near future AVHRR SST received with other HRPT-stations (such as Spain and Ireland) will be available for all HIRLAM member states. This data is almost identical to the current operational AVHRR SST product and therefore the above described assimilation scheme and error statics can easily be applied on this data.

Chapter 5

Impact study

In this chapter the impact study is discussed. Two types of experiments have been performed, one with the conventional SST and the other with the assimilated AVHRR SST, generated as discussed in the previous chapter. The first section describes the experiments. Section 5.2 gives a rough outline of the weather during the experiments. In Section 5.3 the output of both models is verified against synoptic observations. This section is subdivided into parts discussing the impact on five observed physical parameters (pressure, pressure reduced to mean sea level, temperature, dew point temperature and 10 meter wind) and pseudo-observed parameters: latent and sensible heat fluxes above the North Sea. This chapter ends with a summary of the impact results and conclusions.

5.1 Experiments

The region on which the HIRLAM experiment has been performed is shown in the Figure 5.1. In this figure two regions are shown. The large region is the current operational HIRLAM region. The experiments are performed on the small region with boundary values of the large region. The experiment region is roughly a square from Iceland to Corsica, covering the North Sea and part of the North Atlantic Ocean. The region is chosen such that the Netherlands lies in the center of the region and has an overlap with AVHRR coverage of the KNMI receiver. The experiment region has a grid resolution

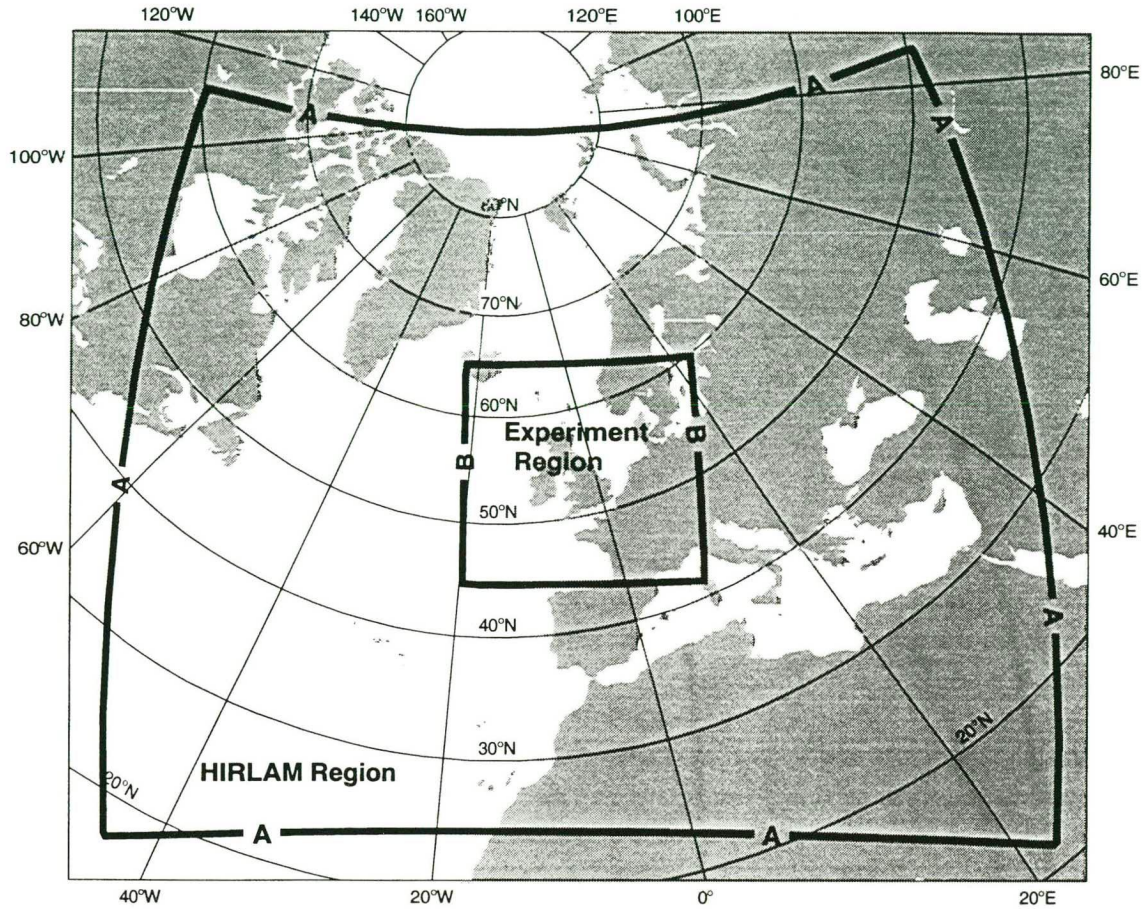

Figure 5.1: The regions of the operational HIRLAM and experiment. The HIRLAM region is used to determine the boundaries of the experiment region. The resolution of the HIRLAM region is 164×130; the experiment region has grid resolution of 110×105 with a grid distance of $20km$.

of 110×105 with 31 levels.

A number of meteorological fields are necessary in order to run a HIRLAM experiment. The actual state of the atmosphere should be known (as well as possible) as well as the surface parameters and atmospheric values at the boundaries of the region. The surface parameters, such as the amount of vegetation, are obtained from a climatological data-set. The state of the

atmosphere at the start of an experiment run is equal to the analysis fields of the operational HIRLAM model. The boundaries are extracted also from the analysis fields of the operational HIRLAM model.

Two types of experiments have been performed, using bilinear interpolation of analyzed fields obtained from the operational HIRLAM-model towards the new grid. The difference between the experiments is the origin of the SST field. One experiment, called reference, contained operational HIRLAM SST. The other experiment has been performed with assimilated AVHRR SST.

The time periods over which the experiments have been run are shown in Table 5.1. Each three hours within this period are taken as starting point for the experiment run. Each run has a forecast length of 12 hours and stores every three hours the state of the atmosphere. The presence of the operational HIRLAM fields is essential in order to run an experiment.

Time Periods of the Experiments		
	start date	end date
Period 1	22/06/1998	04/07/1998
Period 2	01/05/1999	14/05/1999
Period 3	20/09/1999	04/10/1999

Table 5.1: Time periods of the experiments

5.2 Weather and SST during the experiments

By showing the positions of high and low pressure regions and discussing the 10 meter wind in the experiment period an image is made for the weather situation. The difference between reference SST and assimilated AVHRR SST for each period is also discussed. For 6 days in each period the wind and pressure at mean sea level are shown.

5.2.1 June 22 - July 4, 1998

The positions of the high and low pressure regions between June 22 and July 4 are shown in Figure 5.2(a). The pressure and time are shown as sub- and

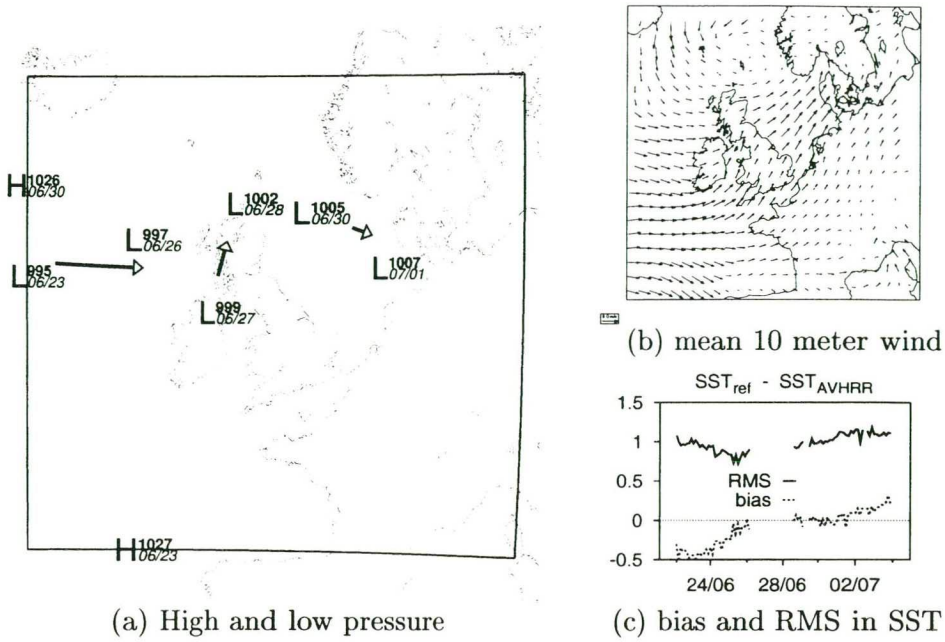

(a) High and low pressure

(b) mean 10 meter wind

(c) bias and RMS in SST

Figure 5.2: (a) Positions of the high and low pressure regions between June 22 and July 4 1998 denoted by H and L. The pressure regions and the border of the experiment region are local maxima or minima of the pressure. Superscript shows the pressure value; subscript the date (month/day); (b) mean 10 meter wind; (c) Bias and root mean square of differences between reference SST and assimilated SST.

superscripts respectively. A low pressure region enters the experiment region south of Iceland and west of Ireland. This low attains a lower pressure and then moves around Scotland towards the North Sea while becoming less deep. At the southern border above the Atlantic Ocean the pressure at sea level is high in the first few days of this period; this region moves north along the edge of the experiment region.

In Figure 5.3 10 meter wind vectors and isobars of the pressure at mean sea level for specific days are shown. The panels show the state of the atmosphere for 6 successive days.

At the start of this period the 10 meter winds above the North Sea are west to south-west and become north-west in the last few days of this period. The mean 10 meter wind is shown in Figure 5.2(b). Strong winds from the west are present above the Atlantic Ocean in the first part of this period, turning

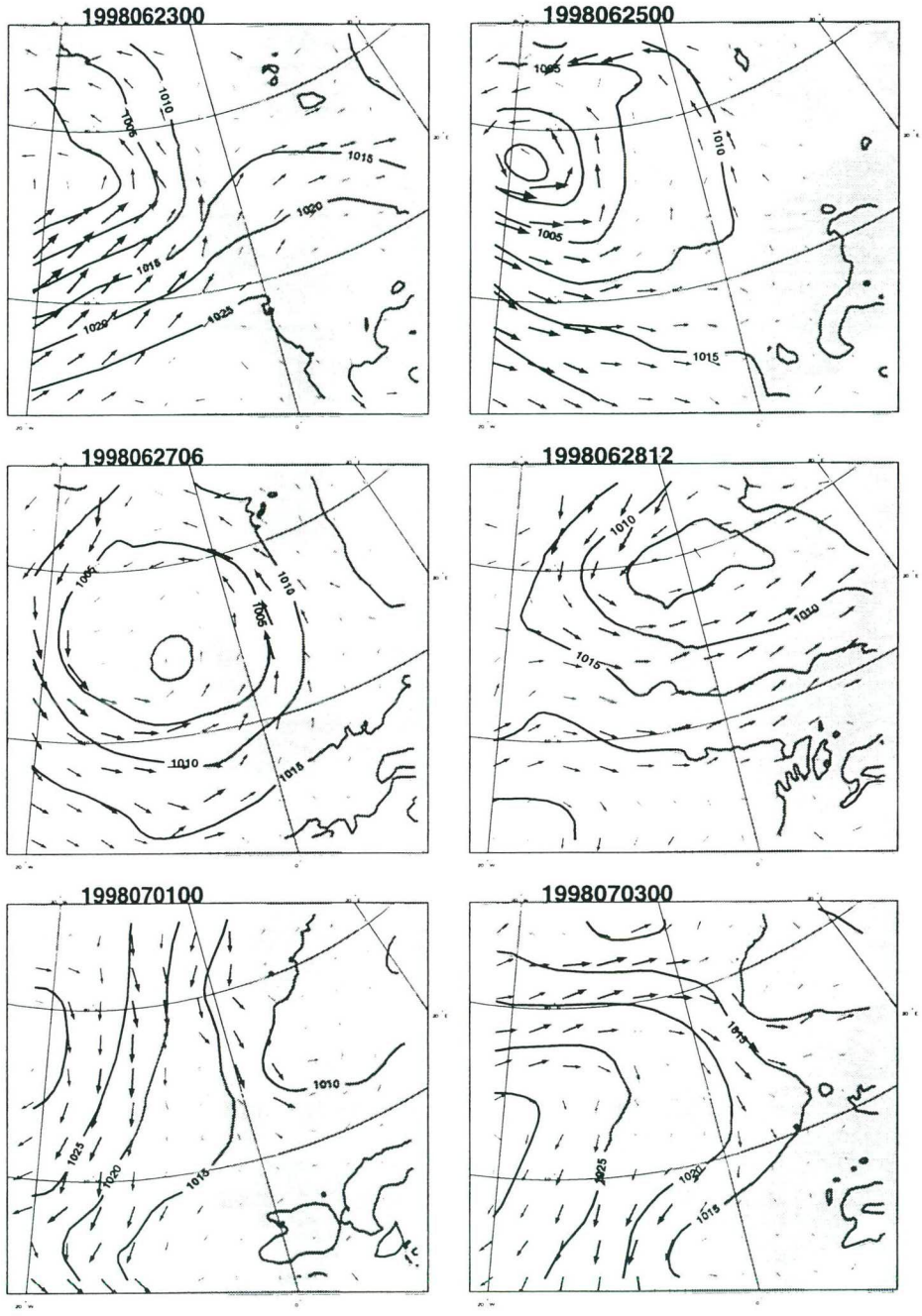

Figure 5.3: 10 meter wind and pressure between June 22 and July 4,1998

to strong winds from the north.

The bias and RMS of the difference between reference SST and assimilated AVHRR SST are shown in Figure 5.2(c). The bias is negative in the first

part of the period: AVHRR SST is higher than reference SST. Within a few days this difference is diminished. The root mean square is around $1K$.

5.2.2 May 1 - May 14, 1999

A high pressure region was present during the first days of the experiment. On the first of May this high is situated west of Ireland. During the following days the pressure in this region increased while it traveled over the British Isles and the North Sea towards Norway. A low pressure region coming from the south-west of Ireland follows a path which lies a little more south with a delay of 7 to 8 days, see Figure 5.4(a).

Figure 5.5) shows the 10 meter wind vectors and mean sea level pressure for 6 days in this period.

Above the North Sea the wind was north-east to east. On the Atlantic Ocean

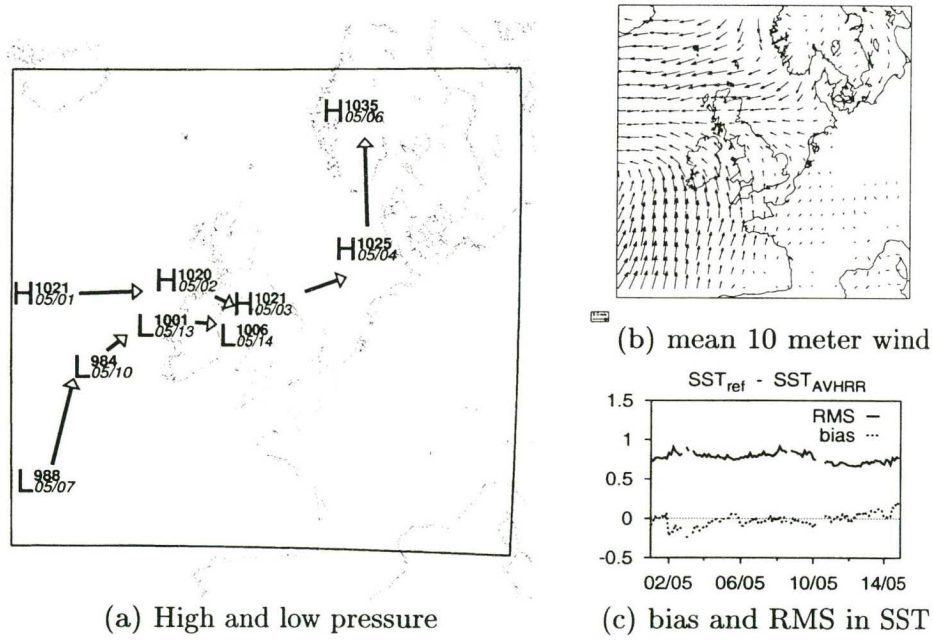

(a) High and low pressure

(b) mean 10 meter wind

(c) bias and RMS in SST

Figure 5.4: a) Positions of the high and low pressure regions between May 1 and May 14 1999.; b) mean 10 meter wind; c) bias and root mean square of differences between reference SST and assimilated SST.

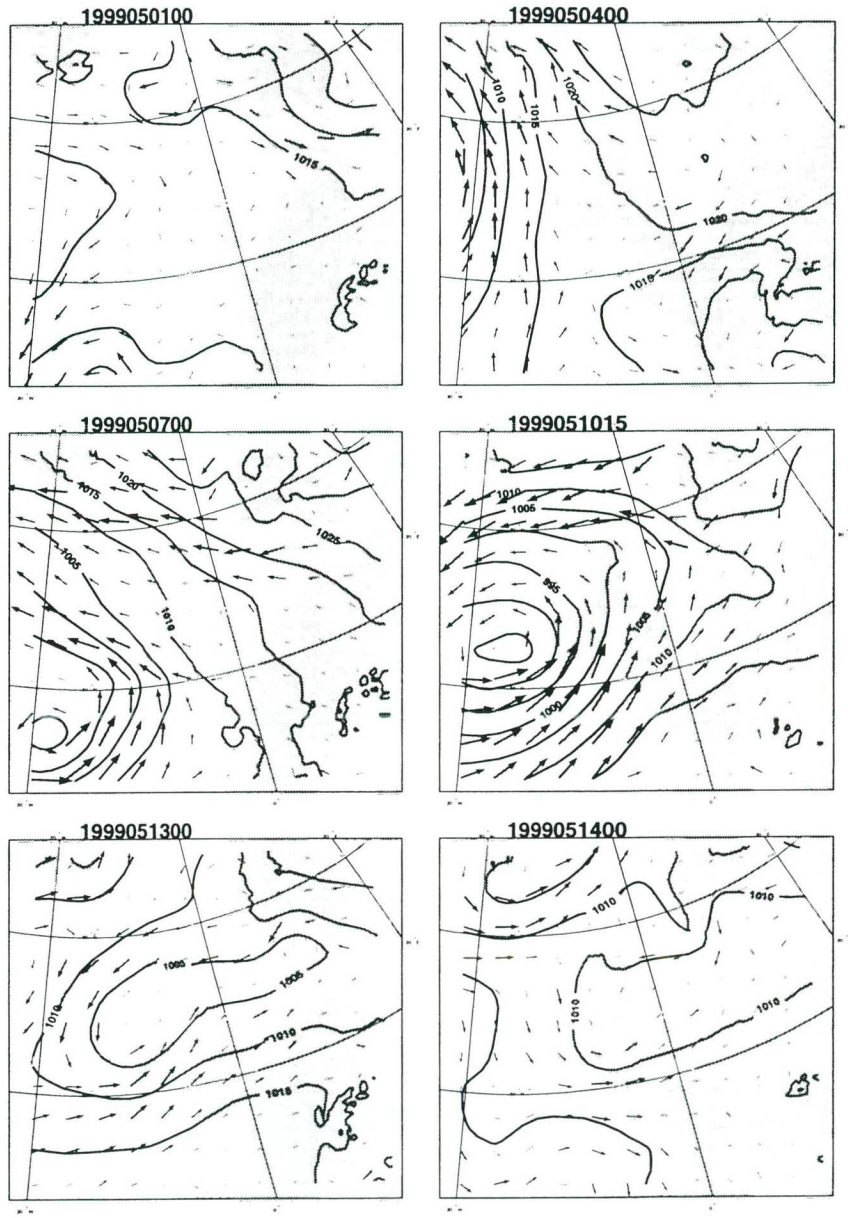

Figure 5.5: 10 meter wind and pressure between May 1 and May 14, 1999

the winds strong coming from south-west to south, see Figure 5.4(b).

From Figure 5.4(c) it can be seen that bias is close to zero and the RMS is nearly constant due to the more detailed SST field when AVHRR SST is concerned.

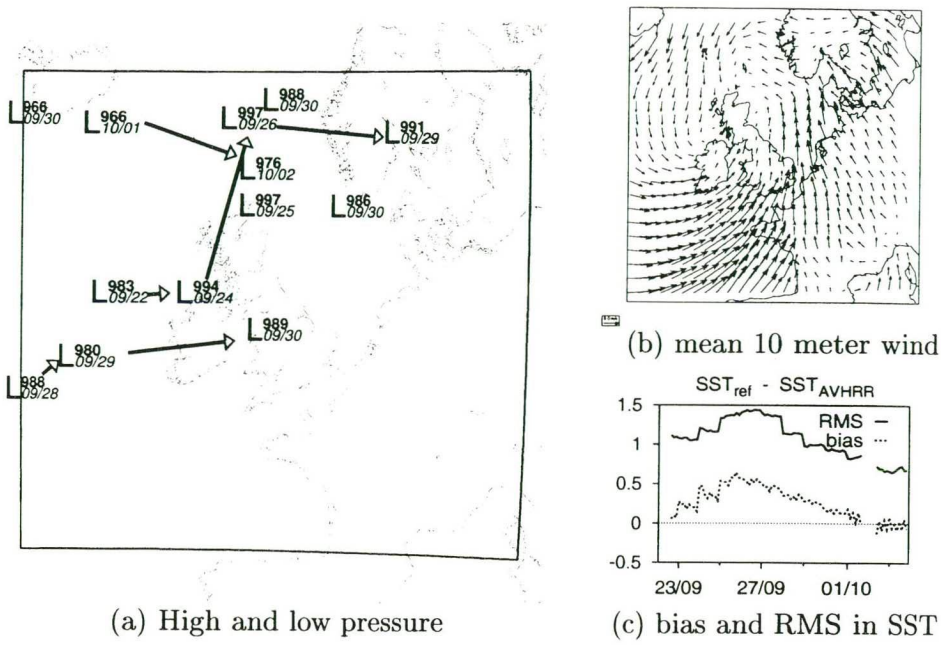

(a) High and low pressure

(b) mean 10 meter wind

(c) bias and RMS in SST

Figure 5.6: a) Positions of the high and low pressure regions between September 22 and October 4 1999; b) mean 10 meter wind; c) bias and root mean square of differences between reference SST and assimilated SST.

5.2.3 September 20 - October 4, 1999

A large number of low pressure zones are present in this period. In the first few days a low lies west of Ireland and travels towards the North Sea. In the second part a very active low enters the experiment region near Iceland and travels rapidly towards the North Sea, see Figure 5.6(a).

Figure 5.7 shows the 10 meter wind vectors and mean sea level pressure for 6 days in this period.

The 10 meter wind above the North Sea is in the first half varying between moderate winds from the north east to weak south east to south west winds In the southern Atlantic strong winds from the west occur and gained speed to the end of the period.

The reference SST is greater than the AVHRR SST (positive bias). The RMS grows to a maximum of $\approx 1.5K$ after which it decreases to ≈ 0.75.

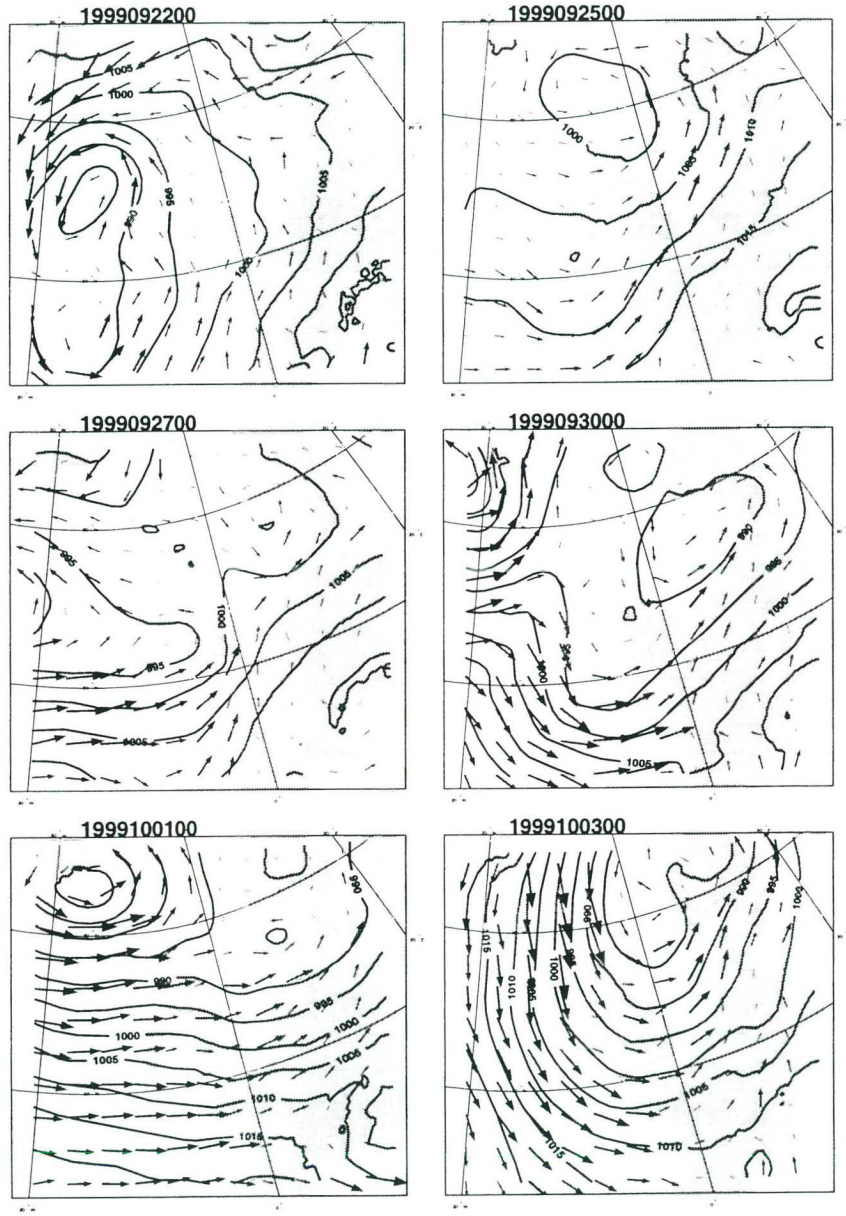

Figure 5.7: 10 meter wind and pressure between September 22 and October 4, 1999

5.3 Impact Results

The model output results are verified against synoptic observations of observed pressure, pressure reduced to mean sea level, 2-meter temperature, 2-meter dew point temperature and 10-meter wind for forecast lengths of 0, 3, 6, 9 and 12 hour. An experiment run with a forecast length of 0 is the output of the model after the first integration step. The results for the different periods and physical parameters are discussed in Sections 5.3.1- 5.3.5. The verification results are presented as changes in root mean square (RMS) of the differences between observed and forecasted values of the five physical parameters. A division is made with respect to all, high and low wind speeds. Wind speeds greater than $4m/s$ are identified as high wind speeds. The impact on heat fluxes above sea are investigated and described in Section 5.3.6 with the same division in wind speeds.

Four verification regions are considered for all verifications shown in Figure 5.8. The four regions are abbreviated as follows: the whole region as all, a region covering Ireland and England as IrE, the region covering Belgium and the Netherlands as BNL and the region in the central North Sea as CNS. Note that CNS lies entirely above sea while BNL is above land. The other

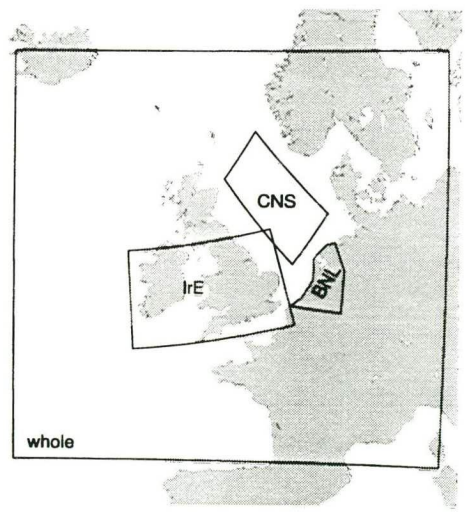

Figure 5.8: The Four Verification regions: the whole region, Ireland and England (IrE), central North Sea (CNS) and Belgium and the Netherlands (BNL).

two regions have both land and sea observations. The impact in the regions BNL and CNS is discussed in the next sections; impact results of all regions are shown in Appendix C.

Observations which are used for assimilation are also used for verification of experiments. Collocation in time (observations within a time window of 1 hour around the forecasting time) and place (using bilinear interpolation of the forecasted fields) are used in the verification.

5.3.1 Observed pressure

The impact on observed pressure in region BNL and CNS are shown in Figures 5.9 and 5.10. In these figures change in RMS is shown for the three experiment periods. The percentile change in RMS for each forecast length is determined by

$$\% \text{ change in } RMS = 100\frac{RMS_{AVHRR} - RMS_{ref}}{RMS_{ref}}. \tag{5.1}$$

When RMS_{AVHRR} is less than RMS_{ref} this value will be negative which is called a positive impact. To verify observed pressure with a forecasted field the height of the observations is important.

Apart from the first period a positive impact is observed for all and high wind speeds. The low wind speed observation show less impact above region BNL. The changes in RMS in the first period show a positive impact for all wind speeds for forecast lengths smaller than or equal to 6 hours due to the positive impact originating from high wind speed observations. Note that the means of the reference RMS (numbers in the left corner of each sub figure) in the first period are higher than those in the other two periods.

In Figure 5.10 the changes in RMS's are shown for the region CNS. Again a positive impact is observed in the second and third period. Note that there were no simultaneous low wind speed and pressure observations in the first and third period above region CNS.

Except for the the first period, RMS's of the observed pressure improve for all wind speeds and forecast lengths.

The mean of both reference and AVHRR RMS's above sea are a factor two

larger than above land, probably due to the fact that a barometer on board of a buoy is less frequently calibrated and checked than one on land.

5.3.2 Observed pressure reduced to mean sea level

Pressure reduced to mean sea level is obtained by diminishing the observed pressure with a factor dependent on the height above sea. In Figures 5.11 and 5.12 the changes in RMS of the pressure reduced to mean sea level are shown. The RMS's in the first period are larger for the experiments with AVHRR SST, except for low wind speed observations above sea. The mean pressure RMS's in the first period are increased by maximal 7% resulting in a mean RMS which is still smaller than the RMS's above sea, this is valid for all high and low wind speeds. The second period shows a neutral impact for pressure reduced to mean sea level. Offshore low wind speed observations in third period show an improvement of the RMS for all forecast lengths. The high wind speed observations have a neutral to negative impact for the 9 and 12 hour forecast. Above land forecasts longer than 3 hours have a negative

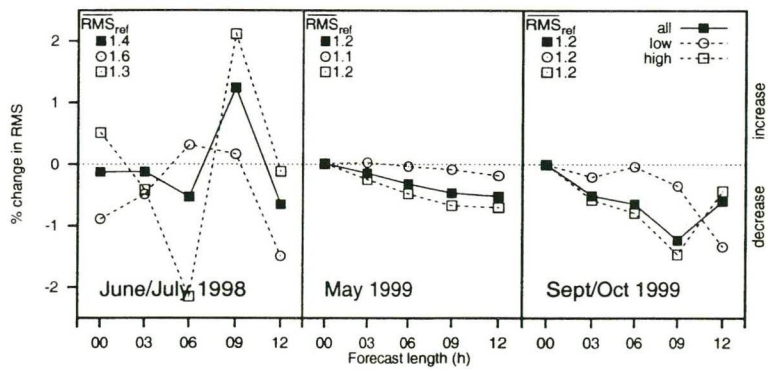

Figure 5.9: Changes in RMS for region BNL of the difference between observed and forecasted pressure for all 5 forecast lengths and three experiment periods. The filled square reflects the RMS of all observations; the open circle represents the RMS of all observations with an observed low wind speed, that is wind speeds less than 4 m/s; the open square represents observations with high wind speeds (greater than 4 m/s). Mean values of the reference RMS are shown in the top corners.

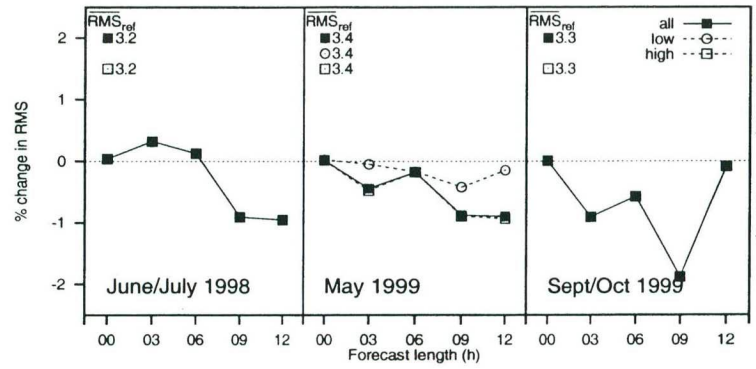

Figure 5.10: Changes in RMS of observed pressure for region CNS. See for more information caption of Figure 5.9.

impact on pressure reduced to mean sea level.

5.3.3 Observed 2-meter temperature

The changes in RMS's for observed 2-meter temperature is shown in Figures 5.13 and 5.14 for regions BNL and CNS respectively.

In region BNL the impact on 2-meter temperature is neutral to positive for the third period. High wind speed observations in the first period show an

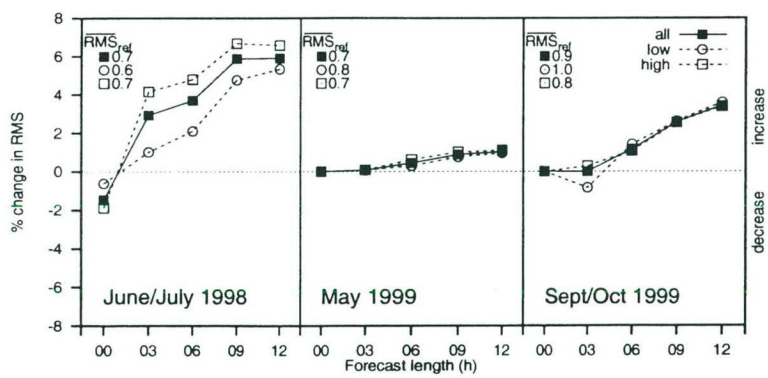

Figure 5.11: Changes in RMS of pressure reduced to mean sea level for region BNL. See for more information caption of Figure 5.9.

increase in RMS while low wind speed observations show a clear decrease in RMS; when all wind speeds are considered a neutral to positive impact is observed for the first period. In the second period a clear positive impact on the RMS's is observed.

For region CNS positive impacts on RMS's are observed in the spring and summer periods, while the autumn period shows a neutral impact for low wind speeds and a negative impact for high wind speeds.

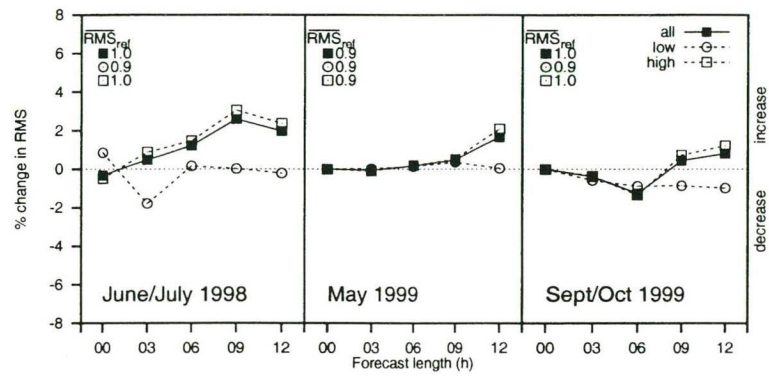

Figure 5.12: Changes in RMS of pressure reduced to mean sea level for region CNS. See for more information caption of Figure 5.9.

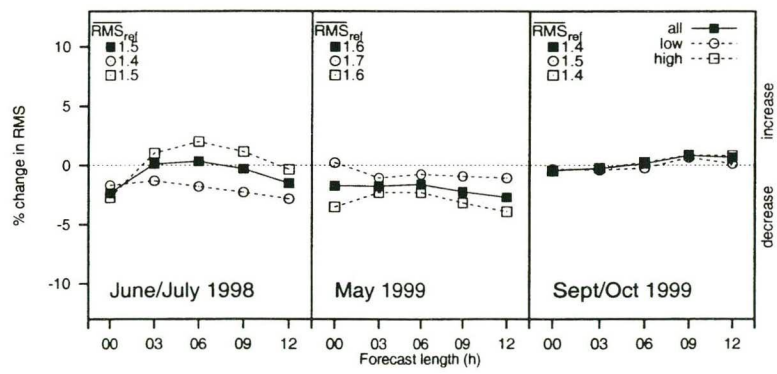

Figure 5.13: Changes in RMS for observed 2-meter temperature in region BNL. See for more information caption of Figure 5.9.

5.3.4 Observed 2-meter dew point temperature

In Figure 5.15 the changes in RMS for the observed dew point temperature is shown for region BNL. RMS's for different wind speeds are similar: moisture above land has a mainly convective origin. In the first period, summer 1998 a negative impact on observed dew point temperature is observed. In the spring of 1999 a positive (lower RMS's) and in the autumn of 1999 a neutral impact is observed in the third period for region BNL.

The impact above sea (region CNS) is shown in Figure 5.16. In the first period a neutral impact is observed, while in the other regions a negative im-

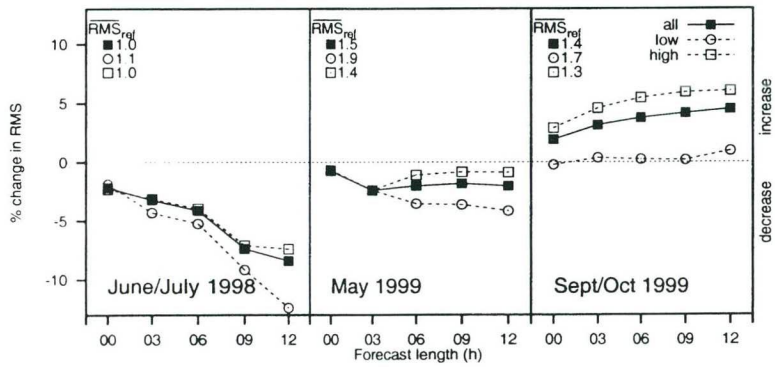

Figure 5.14: Changes in RMS for observed 2-meter temperature in region CNS. See for more information caption of Figure 5.9.

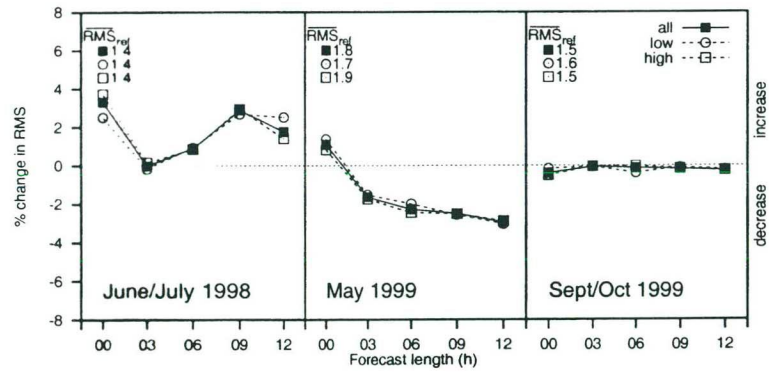

Figure 5.15: Changes in RMS's of dew point temperature for BNL. See for more information caption of Figure 5.9.

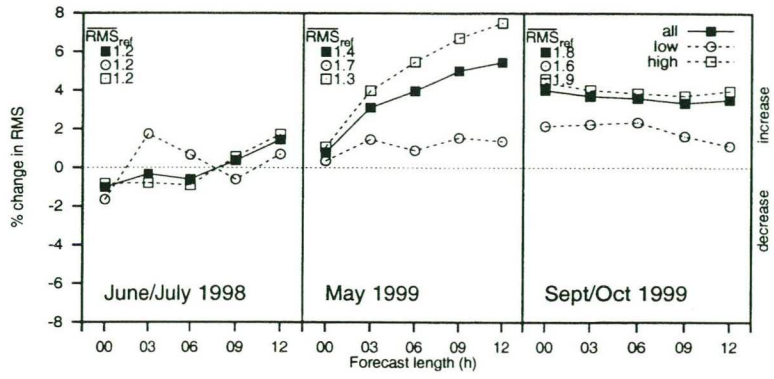

Figure 5.16: Changes in RMS's of dew point temperature for CNS. See for more information caption of Figure 5.9.

pact occurs. Observations with low wind speeds have a less negative impact than observations with high wind speeds.

5.3.5 Observed 10-meter wind vector difference

The wind vector difference is the difference vector between the observed and forecasted wind vector. In Figure 5.17 the RMS of the length of the difference vector for region BNL is shown. Low wind speeds show an increase in RMS in the first two periods and a decrease in the third period. Low winds are varying more with direction and have in general a smaller RMS. The fact that direction for low wind varies easily can be the cause of the negative impact above sea as well as land. High wind speeds above land have a positive impact in the first and third period and a neutral impact in the second period.

Above sea only small positive impact is observed in the third period for all and high wind speeds, see Figure 5.18. In the other periods negative impact dominates.

5.3.6 Simulated heat flux observations above sea

The surface fluxes of heat, water vapor and momentum determine to a great extent the state of the atmospheric boundary layer. As such these fluxes are the principal boundary conditions for NWP models. In principle, the surface

fluxes can be measured. In reality, heat flux measurements are not available.

The O&SI SAF will produce radiative fluxes on a regular bases. These fluxes are downward and net solar surface fluxes and downward longwave radiance, see [O&SI]. These observation can be used as input for the HIRLAM model; the use of these observations is under investigation by DNMI.

At KNMI a number of parameterizations have been developed to estimate the surface fluxes from available routine weather observations (wind, air and water temperature). The difference between the surface temperature and the air temperature determines largely the amount of heat flux. Change in sea surface temperature will result in a change in heat flux.

At KNMI a Fortran routine (called FLXSE1) is developed to calculate surface fluxes, such as sensible and latent heat, over sea by means of the profile method with standard observations as input. Wind speed at a single height, air temperature, dew point temperature and SST have to be specified. See [Beljaars, et al.] for a full description of the routine.

In Figure 5.19 the changes in RMS for the latent heat flux is shown. Latent heat of the sea surface temperature is the amount of heat required to convert 1 unit mass from liquid to vapor without a change in temperature.

In all periods the RMS corresponding to low wind observations are lower than high wind observations, and have more negative impact than high wind observations. This means that for example in the first period both high and

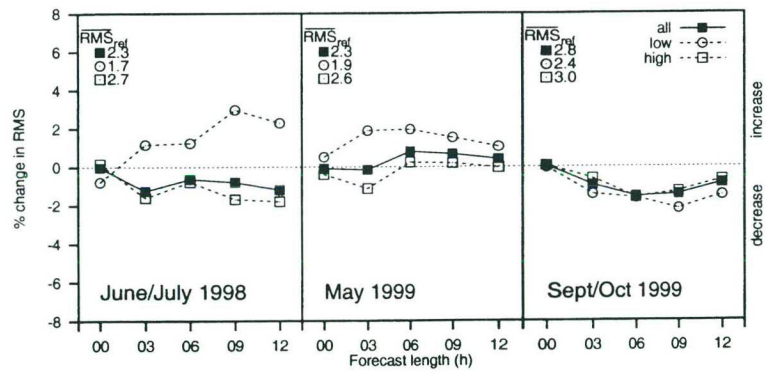

Figure 5.17: Change in 10-meter wind vector difference RMS in region BNL. See for more information caption of Figure 5.9.

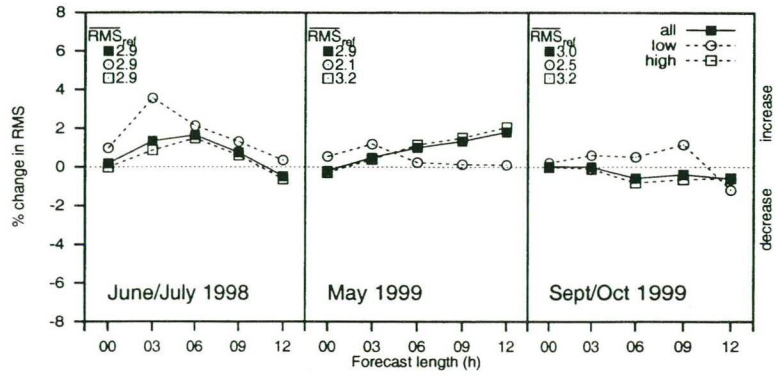

Figure 5.18: Change in 10-meter wind vector difference RMS in region CNS. See for more information caption of Figure 5.9

low wind RMS's increase however in absolute value low wind RMS's remain smaller than high wind RMS's. Only in the second period, May 1999, a positive impact on the latent heat flux is observed, for high wind speeds.

Change in RMS for sensible heat flux is shown in Figure 5.20. Sensible heat is also called enthalpy. The RMS's corresponding to low wind observations are a factor two to three lower than high wind speed RMS's. In the first and third period positive impacts are observed for all, high and low wind speeds, with the exception of the 0 and 3 hour forecast in the first period. The second period shows a neutral to negative impact on all wind speeds and a positive impact on low wind observations.

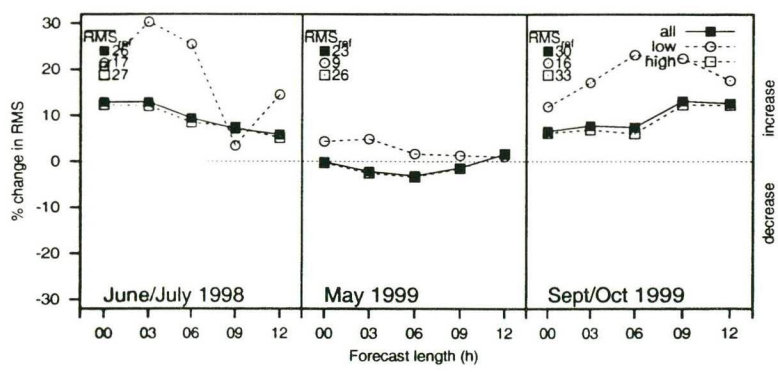

Figure 5.19: Change in latent heat flux RMS in region CNS. See for more information caption of Figure 5.9.

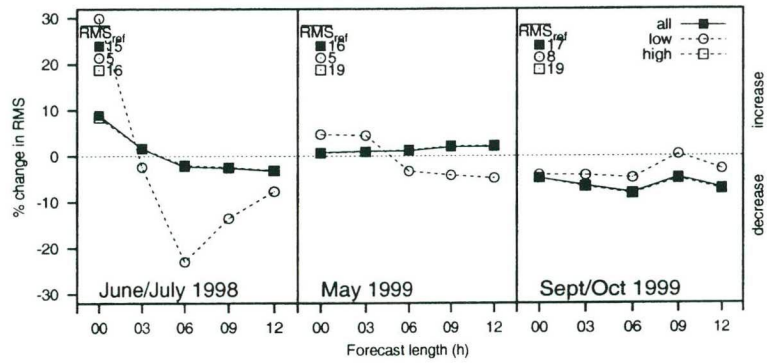

Figure 5.20: Change in sensible heat flux RMS in region CNS. See for more information caption of Figure 5.9.

5.4 Summary and Conclusions

5.4.1 Summary

The largest impacts were observed in 2-meter temperature for both regions in the first two periods, summer 1998 and spring 1999. The sea surface temperature influences the 2-meter temperature more for low wind speeds than high wind speeds. The difference between the observed and 12 hour forecast of the 2-meter temperature in 'de Bilt' for the two experiments in the second period is shown in Figure 5.21. From this figure it can be seen that the difference between observed and forecasted 2-meter temperature of the AVHRR experiment is smaller than the same difference when the reference run is concerned (reduction in the error of about 2%).

The air temperature above sea is known to be closely related to the sea surface temperature for low wind speeds. The change in RMS above sea in the first two periods clearly shows this positive impact.

In the first period the main direction of the wind was east in the experiment region. In this period cold air moved over warm water in regions of low pressure. Because AVHRR SST has more structure, air-sea temperature differences were triggered for low wind speed situations. This resulted in a better forecasted air temperature. Above land air temperature observations during strong wind showed a negative impact.

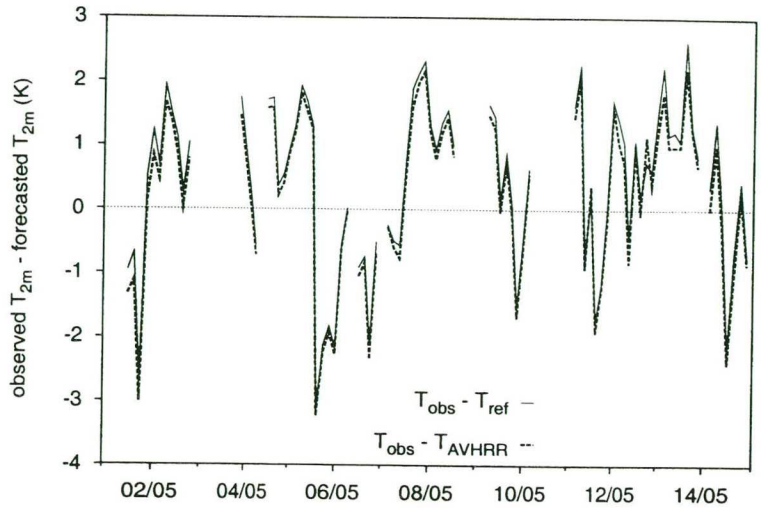

Figure 5.21: Difference between observed and 12 hour forecast of 2-meter temperature in 'de Bilt' for both experiments.

In the second period, spring 1999, the main direction of the wind in the upper part of the experiment region was west while the lower part of the experiment region winds were more coming from the south. The effects on 2-meter temperature RMS's is lower than those in the first period because the effect of replacing the SST is more or less blocked by the direction of the flow.

In the third period a train of low pressure regions was moving from regions near Iceland towards the North Sea. The main wind direction was south-west. The impact on 2-meter temperature for observations during strong winds is negative for this period and neutral for weak winds.

The reference RMS's for 2-meter temperature in the third period are lower than those in the first two periods. In the last period however the RMS's are increased. RMS of the AVHRR experiment attains values comparable to the RMS's of the first two periods (which had a positive impact on RMS's). This is valid for all four regions, see Table C.3.

The use of assimilated AVHRR SST results in an overall improvement in 2-meter temperature for low wind speed conditions. With AVHRR SST the actual RMS's in 2-meter temperature observations are approximately constant for all three period. This is valid for different wind speeds and all

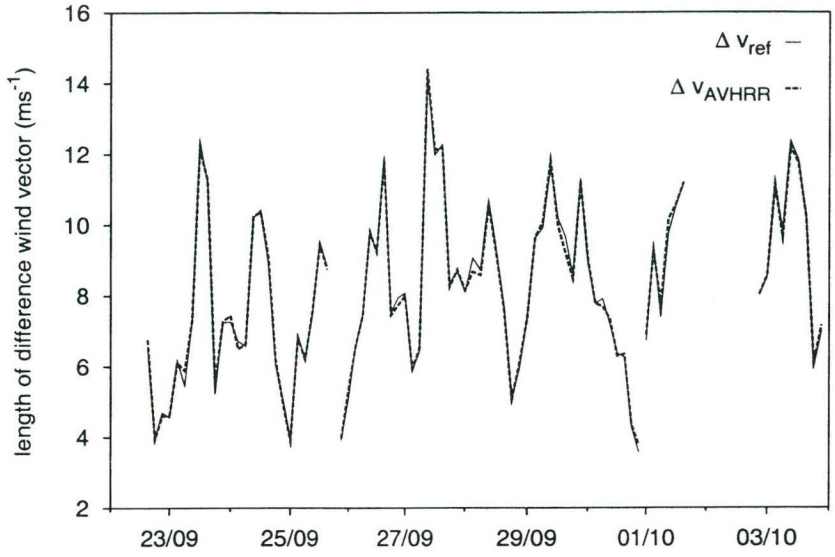

Figure 5.22: 10-meter wind vector difference of both experiments (12 hour forecasts) and wind observations in 'de Bilt'.

regions used in the verification.

Above land forecasted wind vectors with high wind speeds have improved RMS in the first and third period and a neutral change in the second period. The 10-meter wind vector difference between the observed and forecasted wind is shown in Figure 5.22. A small reduction vector difference is achieved when AVHRR SSTs are used.

Above sea the 10 meter wind RMS's in the first period did not show this positive impact. The high winds speed observations above sea in the third period did show a positive impact. Assimilated AVHRR SST results in an overall improvement of strong wind forecast above land, above sea forecasts skills decreases.

Dew point RMS's and pressure RMS's and pressure reduced to mean sea level RMS's had neutral or mixed impact results.

For winds coming from the east the latent heat flux above sea showed a negative impact, while for more westerly winds the impact was positive for high wind speeds. The sensible heat flux above sea clearly profits from AVHRR SST for low wind speeds and all wind speeds and forecast lengths of 6 hour

or more for the more eastward circulation. Sensible heat flux is better forecasted.

5.4.2 Conclusions

Surface fluxes are important physical quantities which determine to a great extent the atmospheric boundary layer. The governing equations in a boundary layer of a NWP model are different from those which simulate change of atmospheric state in the upper atmosphere. For example, horizontal turbulence mixing is modeled in the boundary layer but not in the upper layers.

HIRLAM forecasts of sensible heat fluxes made using AVHRR SST are more consistent with simulated sensible heat flux observations than the reference HIRLAM run. The energy exchange for forecasts using AVHRR SST in the lower boundary, due to the better sensible heat flux, has a closer resemblance to actual energy exchange.

A better description of the heat fluxes results in a better direct forcing of the model. Temperature at 2-meter and 10-meter wind can be seen as the response of the boundary layer model to the change in description of the sensible heat fluxes. The fact that these parameters show an ambiguous impact above sea is probably related to the approximation of the governing equations in the boundary layer. Within the HIRLAM community it is known that the boundary layer needs attention and in the HIRLAM-5 project actions are taken to improve the boundary layer description.

Chapter 6

Conclusions and remarks

In this report the operational AVHRR SST product at KNMI has been investigated upon usefulness for NWP models.

First, validation was conducted by comparing these remotely sensed SST with in-situ buoy and ship measurements. In four fortnight periods data sets of in-situ measurements were prepared to diminish wrong in-situ observations.

The AVHRR SST product is a cloud cleared composite of AVHRR scans over a composite period. A statistical algorithm is developed to detect semi transparent or low cloud contamination of the composites. The validation data gathered in the four validation periods showed that composites updated daily with a composite period of 7 days are favorable above other composites. The mean overestimation is greater for longer periods, however in short period composites the root mean square error is greater. The latter is due to cloud contaminated pixels which leads to underestimations of the actual SST by the remotely sensed SST. In general the bias of AVHRR compositions over 7 days are positive; compositions over 3 days have negative bias.

The daily updated seven-day AVHRR SST composite has generally a better coverage than the three-day composite. Furthermore the root mean square error is minimal for the seven-day daily updated composite when compared to seven-day weekly and three-day daily updated composites.

Error statistics were derived based on a four year data set of weekly AVHRR SST composites. Correlations in this data set are used to fit correlation

functions. Correlations between two locations are found to be dependent on distance, time of the year and the geographical location of the sea. An assimilation scheme based on the optimal interpolation technique, was developed to prepare AVHRR SSTs for use in HIRLAM. Correlation functions form the core of this assimilation scheme.

HIRLAM runs were performed in three periods, each of approximately 14 days. Impact analysis has been performed by verifying forecasts with synoptic observations and simulated observations of latent and sensible heat flux.

A reduction of the error in 2-meter temperature is observed in two of the three periods. In the other period, AVHRR SST had a neutral impact on the 2-meter temperature above land and a negative impact for observations with strong wind above sea. Allthough the RMS's grow in this last period the values are of the same order as in the other period where a reduction of the RMS's was observed. Especially 2 meter temperature forecasts during low wind situations benefit from assimilated AVHRR SST.

Above land forecasted wind vectors with high wind speeds have improved RMS in two of the three experiment periods and a neutral change in the other period. Assimilated AVHRR SST results in an overall improvement of strong wind forecast above land, above sea forecasts skills decreases.

Dew point RMS's and pressure RMS's and pressure reduced to mean sea level RMS's had neutral or mixed impact results.

HIRLAM forecasts of sensible heat fluxes made using AVHRR SST are more consistent with simulated sensible heat flux observations than the reference HIRLAM run. The energy exchange for forecasts using AVHRR SST in the lower boundary, due to the better sensible heat flux, has a closer resemblance to actual energy exchange. Sensible heat flux is better forecasted, using AVHRR SST, for low wind speeds in all three periods. For high wind situations a neutral to positive impact is observed.

Forecasted latent heat flux showed a negative impact in two of the three periods.

A better description of the heat fluxes results in a better direct forcing of the model. Temperature at 2 meter and 10-meter wind can be seen as the response of the boundary layer model to the change in description of the sensible heat fluxes. The fact that these parameters show an ambiguous

impact above sea is probably related to the approximation of the governing equations in the boundary layer.

Investigation and improvement of the boundary layer description of HIRLAM can enlarge the impact of the use of assimilated AVHRR SST. Because within HIRLAM-5 the boundary layer is being improved, implementation of AVHRR SST in the assimilation scheme is recommended, keeping in mind that in the near future the coverage in space and time of high quality AVHRR SST observations will increase.

Additional to the fact that HIRLAM will profit from assimilated AVHRR SST, the users of the current operational AVHRR SST product of KNMI will also benefit from a better SST field.

6.1 Outlook

The assimilation scheme described in this report is, with some adjustments applicable to the forthcoming Ocean & Sea Ice SAF SST product. The large coverage (the whole North Atlantic Ocean), high quality (RMS $\approx 0.5K$) and high resolution ($10km$) will have an strong added value to the current operational AVHRR SST product. In 2001 these products will be operationally available for the European meteorological society. For more information on the Ocean & Sea Ice SAF (see for more information and examples of the products *http://www.meteorologie.eu.org/safo/*).

In the near future AVHRR SST received with other HRPT-stations (such as Spain and Ireland) will be available for all HIRLAM member states. This data is almost identical to the current operational AVHRR SST product and therefore the above described assimilation scheme can easily be applied on this data.

The large coverage and high quality of these new AVHRR SST observations together with the assimilation scheme described in this report will result in a high quality SST field which covers the North Atlantic completely (when SAF products are available). When only shared AVHRR observations are present, assimilation of these observations results in an SST product with a lower boundary which is 10 degrees more south and a left boundary 15 degrees more west than the current operational AVHRR SST product.

Bibliography

[Anderson, et al.] Anderson, S., A. Brisson, S. Eastwood, P. Le Borgne, A. Marsouin (1998) "Developments on SST retrieval over the Atlantic using Geostationary and Polar Orbiter Satellite Data in the Frame of the EUMETSAT Ocean and Sea Ice Satellite Application Facility", *In proceedings of the 9th Conference on Satellite Meteorology and Oceanography, Paris, France*

[Beljaars, et al.] Beljaars, A.C.M., A.A.M. Holtslag, R.M. van Westrhenen (1989) "Discription of a software library for the calculation of surface fluxes" *Royal Netherlands Met. Institute Technical Report.***TR-122**

[Candy & Anderson] Candy, B., S. Andersen (1999) "Evaluation of Skin-Bulk Sea Surface Temperatures Difference Models for use in the Ocean and Sea Ice SAF" *Danish Met. Institute Technical Report*, **99-14**

[Daley] Daley, R., (1991) "Atmospheric data analysis", Cambridge atmosph. and space science series, Cambridge University Press.

[Derber] Derber, J.C. "Assimilation of TOVS data at NMC", *Proceedings of the Seminar on Developments in the Use of Satellite Data in Numerical Weather Prediction,ECMWF, Reading, U.K.*, pp 3-18

[Llewellyn-Jones et al.] Llewellyn-Jones, D.T., P.J. Minnett, R.W. Saunders and A.M. Zavody, (1984), "Satellite multichannel infrared measurements of sea surface temperature of the N.E. Atlantic Ocean using AVHRR/2",*Quarterly Journal of the Royal Meteorological Society*, **no.110**, pp 613-631.

[Numerical Recipes] Press, W.H. (1986) "Numerical Recipes", Cambridge University Press

[O'Carroll & Candy] O'Carroll, A.G., B. Candy (1999) "Generation of high resolution Sea Surface Temperature observations from AVHRR satellite data for use in the mesoscale SST analysis", *UK Met. Office Forecasting Research Technical Report*, **No. 228**.

[O&SI] Ocean and Sea Ice SAF project team, "Ocean and Sea Ice Satellite Application Facility Software Requirements Document", December 1998

[Reynolds & Smith] Reynolds, R. W. and T. M. Smith, (1994) "Improved global sea surface temperature analyses",*J. Climate*, **7**, pp 929-948.

[Saunders & Kriebel] Saunders, R.W. and K.T. Kriebel, (1988) "An improved method for detecting clear sky and cloudy radiances from AVHRR data", *International Journal of Remote Sensing*, **Vol.9**, no.1, pp 123-150.

Appendix A

Influence of cold/warm water fronts on S^2

Here the influence of a cold/warm water front on the sample standard deviation is investigated. Assume a warm/cold waterfront exists around the origin in an area A which is a square $(-b, b)^2$, with the following piecewise linear temperature profile with a temperature difference equal to ΔT and a base temperature level of T_0:

$$T_{a,\delta}(x,y) = \begin{cases} T_0 & -b \leq x < a - \frac{1}{2}\delta \\ T_0 + \left(\dfrac{2x - 2a + \delta}{\delta}\right)\Delta T & a - \frac{1}{2}\delta \leq x < a + \frac{1}{2}\delta \\ T_0 + \Delta T & a + \frac{1}{2}\delta \leq x < b \end{cases} \tag{A.1}$$

Figure A.1 shows this temperature profile; the position of the front is at $x = a$ and the transient region has thickness δ. The mean temperature over the region A is

$$\bar{T} = \frac{1}{A}\int_A T_{a,\delta}(x,y)dA = T_0 + \frac{1}{2}\Delta T\left(1 - \frac{a}{\delta}\right), \tag{A.2}$$

while the standard deviation is equal to

$$\sigma^2_{a,\delta} = \frac{1}{A}\int_A \left(T_{a,\delta}(x,y) - \bar{T}\right)^2 dA = \frac{\Delta T^2}{4}\left(1 - \frac{a^2}{b^2} - \frac{\delta}{3b}\right). \tag{A.3}$$

Suppose that the N measured AVHRR SST values T_i are nicely distributed over the region A, then the sample standard deviation S^2, for N large enough,

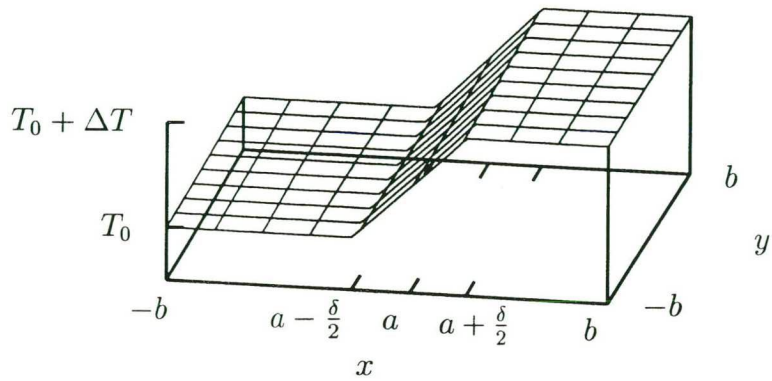

Figure A.1: The temperature profile $T_{a,\delta}(x, y)$.

is approximately equal to $\sigma^2_{a,\delta}$, that is

$$S^2 \approx \frac{\Delta T^2}{4}\left(1 - \frac{a^2}{b^2} - \frac{\delta}{3b}\right). \tag{A.4}$$

Suppose there is a slow front present in the region A that is $a = 0$ and $\delta = 2b$, then the sample standard deviation becomes:

$$S^2 \approx \frac{\Delta T^2}{12} \tag{A.5}$$

When S^2_{TH} is the threshold value then the slow fronts with a difference in temperature satisfying

$$\Delta T < \sqrt{12 S^2_{TH}} \tag{A.6}$$

will generally still be estimated correctly.

For a very steep front the value of δ is minimal half a pixel, that is approximately $1km$. The largest value for S^2 in this case is when $a = 0$. Therefore a steep front with a temperature difference which satisfies

$$\Delta T < 2\sqrt{\frac{3b}{3b-1} S^2_{TH}} \tag{A.7}$$

will generally still be estimated correctly.

The values of S_{TH}^2 and b determine the correctness of the AVHRR SST. In the validation below b is taken to be $18km$ and S_{TH}^2 is 2.0. Using these values slow fronts with a temperature difference of $4.9K$ and steep fronts with a temperature difference of $2.9K$ are recognized. It is of major importance that the number of measured SST in A is large enough, otherwise the statistical justification collapses.

Appendix B

Autocorrelation of weekly AVHRR images

B.1 Seasonal autocorrelation

Over a four year period the autocorrelation is calculated. The seasonal influence on the autocorrelation is investigated for the North Sea, the Baltic Sea, the Mediterranean Sea, the Black Sea and the Atlantic Ocean. Additionally, for the Atlantic Ocean the latitude dependence of the autocorrelation is examined by selecting two latitude bands. The five regions are shown in Figure 4.1 on page 26.

In Figures B.1(a)-(d) and B.2(a) and (b), four lines are shown, denoting the autocorrelation in $50km$ bins for four seasons. In the lower part of the graphs the standard deviations of the autocorrelations in these bins are shown.

The correlation in winter (dotted line numbered 4) has the steepest decay for small distances and all five regions. The corresponding standard deviation for winter correlation has high values with respect to correlations at equal distances in other seasons, although in the Baltic Sea the standard deviations is not clearly the highest. This can be caused by the fact that deep waters are less cooled than shallow waters or the occurrence of ice in high latitude seas. In the Atlantic Ocean a strong temperature gradient exists near the Warm Gulf stream which will result in a lower correlation over larger distance than

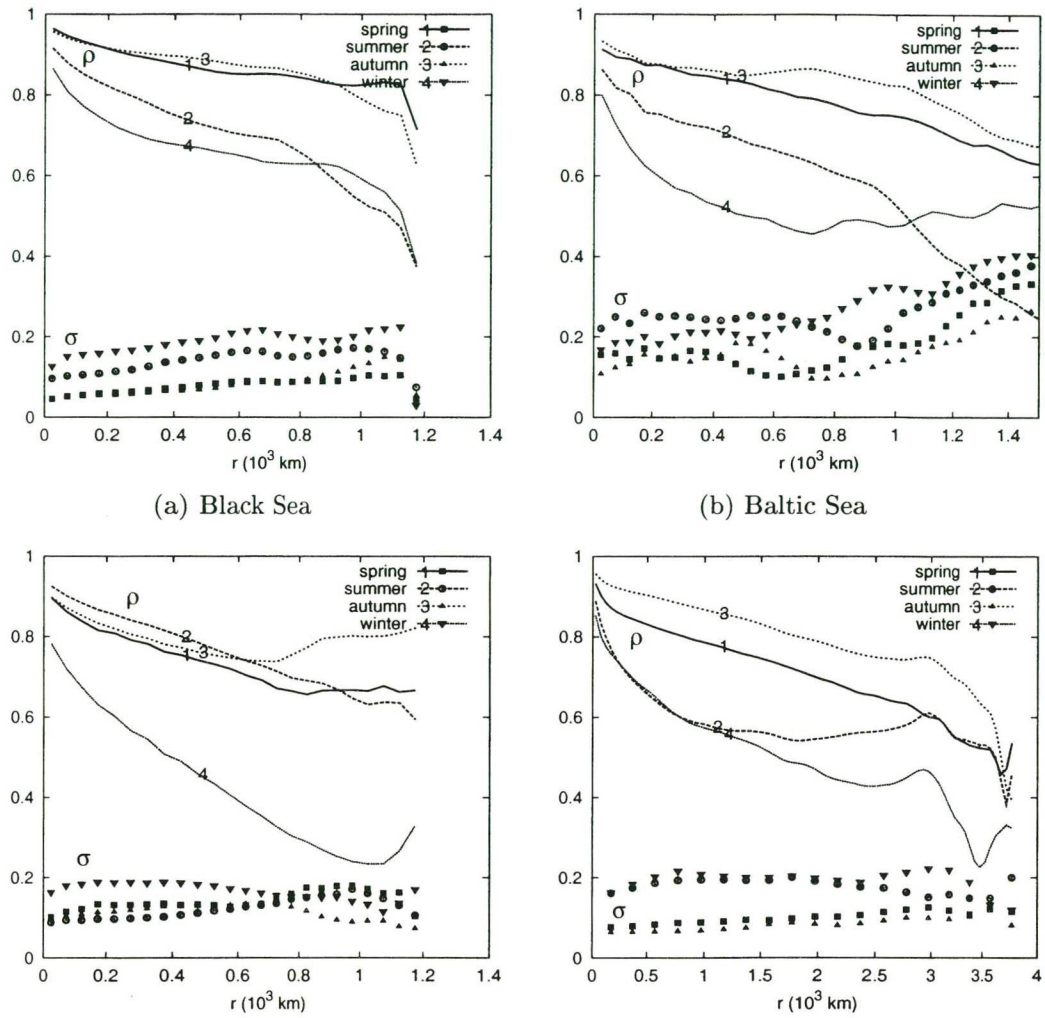

(a) Black Sea

(b) Baltic Sea

(c) North Sea

(d) Mediterranean Sea

Figure B.1: Autocorrelation with respect to the seasons for the Black Sea, the Baltic Sea, the North Sea and the Mediterranean Sea.

when the gradient does not appear. The low winter correlations are most obvious in the North and the Baltic Sea.

During spring the sun heats up the water surface (solid line numbered 1). This heating can be locally and the energy is transported only slowly over several kilometers. The correlation in this season is higher than the correlation in winter.

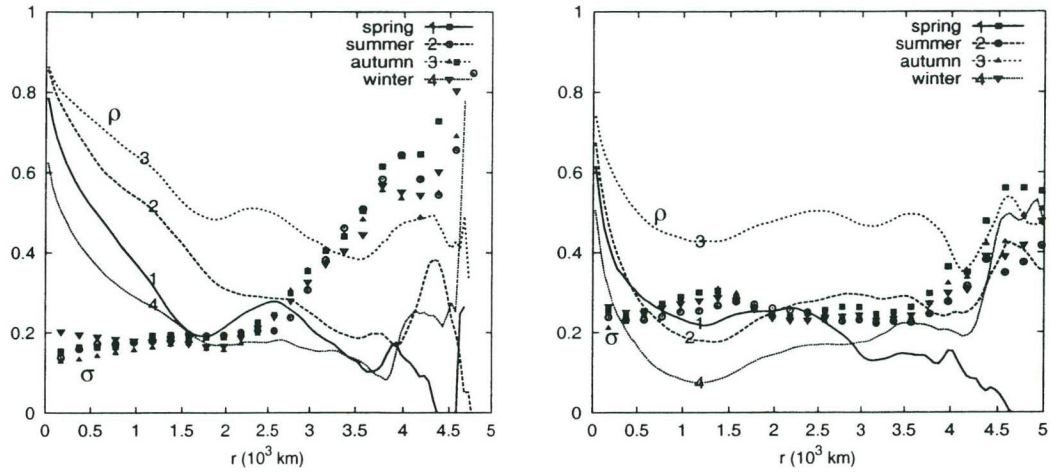

(a) Atlantic Ocean: 40° - 50° (b) Atlantic Ocean: 60° - 70°

Figure B.2: The autocorrelation versus the distance of AVHRR SST in the Atlantic Ocean for latitudes between (a) 40° and 50° and (b) 60° and 70°.

The autocorrelation in the Mediterranean Sea during summer has a similar graph as the autocorrelation during winter. The water surface has heated up already during spring, however locally there can occur some 'hot-spots' because of extensive heating of the water surface: a lower autocorrelation. This is probably also the case in the southern part of the Atlantic Ocean (see Figure B.2(a)) and thus influences the graph of autocorrelation in this season.

Autumn shows the highest correlations. The sun has heated the water surface during spring and summer and the energy is spread around the seas due to mixing of the upper water level by storms.

In Figure B.2 the AVHRR SST have a lower correlation for distances between 500 and 2000 km for latitudes between northern latitude range for all seasons than for the southern range of latitudes. The graphs of the correlations in Figure B.2 have a steeper decay for the northern latitudes. This is possibly due to sharp temperature gradients near the warm current or near ice edges. For both latitude ranges winter correlations have the lowest values while autumn correlations have the highest values.

B.2 Horizontal distribution of autocorrelation

The autocorrelations in the previous section were only investigated with respect to distance and season. The assumption that autocorrelations are direction independent is founded in this section.

In Figure B.3 contour plots of the horizontal distribution of the autocorrelation are shown. The autocorrelation here is calculated using the whole four year period thus including all four seasons. Furthermore no latitude bands are used for the Atlantic Ocean. The relative positions of two points are calculated by determining the angle between the vector along the earth surface from one position to the other and the northern direction. The distance is in kilometers on the both axes.

The influence of the shape of the sea is clearly visible for the Black Sea, see Figure B.3(a). The contour of values of 0.95 follows the coast line. In Figure B.3(b), the Baltic Sea, these coast effects are less visible. The autocorrelation values are less nicely distributed over this region compared to other regions. This is most likely due to the shape of the sea. The spatial autocorrelation in the North Sea, see Figure B.3(c) has a direction indepen-

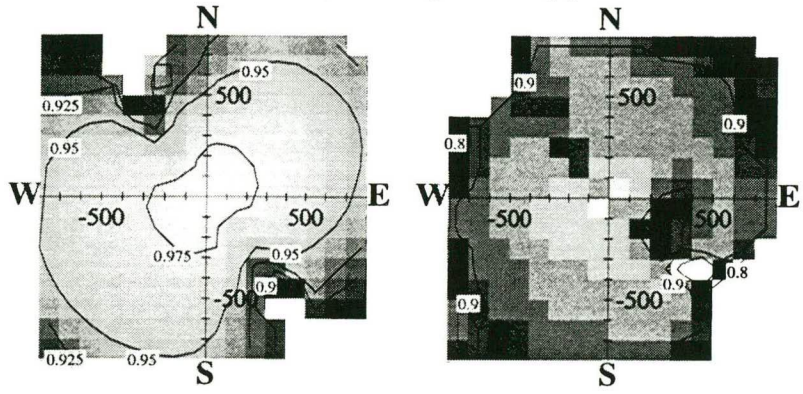

(a) Black Sea, 20 km from coast

(b) Baltic Sea, 20 km from coast

Figure B.3: The two dimensional distribution of the AVHRR autocorrelation over the whole period for the five different regions (see also next page). Note that the scales of plots (a),(b) and (c) differ from (d) and (e): the Mediterranean Sea and the Atlantic Ocean have scales twice as large as the others.

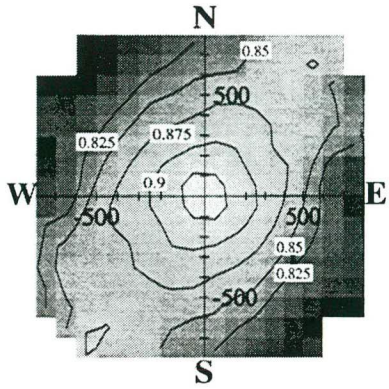

(c) North Sea

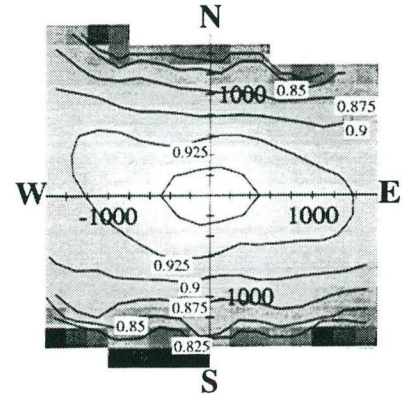

(d) Mediterranean Sea

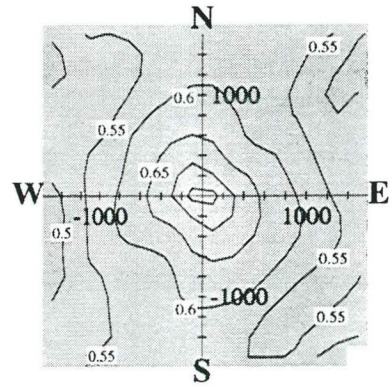

(e) Atlantic Ocean

Figure B.3: (continued)

dent contour of values of 0.9, however contour lines with lower values show a NE-SW independence caused by the fact that the Atlantic Ocean lies north-easterly of the North-Sea. The spatial autocorrelation in the Mediterranean Sea, see Figure B.3(d) follows roughly the shape of the sea. The contour of values of 0.95 is almost direction independent. For the Atlantic Ocean (Figure B.3(e)) the contour lines at distances smaller than 1000km are direction almost independent.

In general the autocorrelation depends only on the distance (and season) when distances are smaller than 500 km for the three small regions and 1000 km for the two large regions. Directional influences can be neglected.

Appendix C

Impact results

In this appendix all changes in RMS for four observed physical quantities are shown in tables. Each table is divided into three subtables representing the results for all, low and high wind speeds. The reference value (abbreviated as ref) is the RMS of verification of the physical quantity for the reference run for corresponding region and forecast length. The numbers in italic are the change in percentage of the reference RMS. This change is calculated using the reference RMS and RMS of the verification using forecast with AVHRR SST:

$$\text{prec. change in RMS} = 100\frac{RMS_{AVHRR} - RMS_{ref}}{RMS_{ref}}. \tag{C.1}$$

observed pressure											
June 22 - July 4, 1998											
		Forecast lengths									
		00		03		06		09		12	
wind	Region	ref	%	ref	%	ref	%	ref	%	ref	%
all	whole	1.9	*-0.1*	1.9	*-0.2*	1.9	*-0.3*	1.9	*-0.1*	1.9	*-0.1*
	BNL	1.4	*-0.1*	1.4	*-0.1*	1.4	*-0.5*	1.4	*1.2*	1.3	*-0.7*
	CNS	3.3	*0.0*	3.3	*0.3*	3.2	*0.1*	3.2	*-0.9*	3.1	*-0.9*
	IrE	2.1	*0.1*	2.1	*0.0*	2.1	*0.1*	2.2	*0.6*	2.2	*0.5*
low	whole	1.9	*0.0*	1.9	*-0.2*	1.9	*-0.1*	1.9	*0.1*	1.9	*-0.1*
	BNL	1.5	*-0.9*	1.7	*-0.5*	1.6	*0.3*	1.5	*0.2*	1.5	*-1.5*
	CNS	3.4	*-0.1*	-	-	-	-	-	-	-	-
	IrE	1.8	*0.4*	1.9	*0.3*	2.0	*0.6*	2.2	*-0.1*	2.2	*0.8*
high	whole	1.8	*-0.3*	1.9	*-0.2*	1.9	*-0.6*	1.9	*-0.4*	1.9	*-0.2*
	BNL	1.2	*0.5*	1.3	*-0.4*	1.3	*-2.1*	1.3	*2.1*	1.3	*-0.1*
	CNS	3.3	*0.0*	3.3	*0.3*	3.2	*0.1*	3.2	*-0.9*	3.1	*-0.9*
	IrE	2.2	*0.1*	2.1	*0.0*	2.1	*0.0*	2.2	*0.8*	2.2	*0.4*
May 1 - May 14, 1999											
p		Forecast lengths									
		00		03		06		09		12	
wind	Region	ref	%	ref	%	ref	%	ref	%	ref	%
all	whole	1.8	*0.0*	1.9	*0.0*	1.9	*-0.1*	1.9	*-0.2*	1.9	*-0.3*
	BNL	1.0	*0.0*	1.2	*-0.1*	1.2	*-0.3*	1.2	*-0.5*	1.2	*-0.5*
	CNS	3.5	*0.0*	3.4	*-0.4*	3.3	*-0.2*	3.3	*-0.9*	3.3	*-0.9*
	IrE	2.2	*0.0*	2.2	*0.1*	2.2	*0.0*	2.2	*0.4*	2.2	*-1.1*
low	whole	1.9	*0.0*	1.9	*0.0*	1.9	*0.1*	1.9	*-0.2*	1.9	*-0.1*
	BNL	1.0	*0.0*	1.1	*0.0*	1.1	*0.0*	1.1	*-0.1*	1.1	*-0.2*
	CNS	3.2	*0.0*	3.4	*-0.1*	3.6	*-0.2*	3.2	*-0.4*	3.4	*-0.1*
	IrE	2.2	*0.0*	2.2	*0.0*	2.2	*0.2*	2.2	*-0.4*	2.3	*-0.8*
high	whole	1.8	*0.0*	1.9	*-0.1*	1.9	*-0.2*	1.9	*-0.1*	1.9	*-0.5*
	BNL	1.1	*0.0*	1.2	*-0.2*	1.2	*-0.5*	1.2	*-0.7*	1.2	*-0.7*
	CNS	3.5	*0.0*	3.4	*-0.5*	3.3	*-0.2*	3.3	*-0.9*	3.3	*-0.9*
	IrE	2.2	*0.0*	2.2	*0.2*	2.2	*-0.1*	2.1	*0.8*	2.2	*-1.2*
September 20 - October 4, 1999											
p		Forecast lengths									
		00		03		06		09		12	
wind	Region	ref	%	ref	%	ref	%	ref	%	ref	%
all	whole	1.8	*0.0*	1.9	*-0.3*	1.9	*-0.2*	1.9	*-0.2*	1.9	*-0.1*
	BNL	1.0	*0.0*	1.2	*-0.5*	1.2	*-0.6*	1.2	*-1.2*	1.3	*-0.6*
	CNS	3.5	*0.0*	3.4	*-0.9*	3.3	*-0.6*	3.2	*-1.9*	3.1	*-0.1*
	IrE	2.2	*0.0*	2.2	*-0.6*	2.2	*-0.1*	2.2	*-0.2*	2.2	*-0.2*
low	whole	1.9	*0.0*	1.9	*-0.3*	2.0	*-0.1*	2.0	*-0.1*	2.0	*0.0*
	BNL	0.9	*0.0*	1.2	*-0.2*	1.3	*0.0*	1.3	*-0.3*	1.3	*-1.3*
	CNS	-	-	-	-	-	-	-	-	-	-
	IrE	2.4	*0.0*	2.4	*-0.6*	2.3	*0.2*	2.3	*0.0*	2.3	*0.3*
high	whole	1.8	*0.0*	1.9	*-0.3*	1.9	*-0.3*	1.9	*-0.3*	1.9	*-0.2*
	BNL	1.0	*0.0*	1.2	*-0.6*	1.2	*-0.8*	1.2	*-1.5*	1.3	*-0.4*
	CNS	3.5	*0.0*	3.4	*-0.9*	3.3	*-0.6*	3.2	*-1.9*	3.1	*-0.1*
	IrE	2.1	*0.0*	2.1	*-0.5*	2.1	*-0.2*	2.1	*-0.2*	2.2	*-0.5*

Table C.1: RMS and change in RMS (in %) in the difference between forecasted and predicted observed pressure.

pressure reduced to mean sea level											
June 22 - July 4, 1998											
		Forecast lengths									
		00		03		06		09		12	
wind	Region	ref	%	ref	%	ref	%	ref	%	ref	%
all	whole	0.8	*-0.2*	0.8	*0.1*	0.9	*1.1*	0.9	*2.3*	0.9	*2.4*
	BNL	0.6	*-1.5*	0.6	*2.9*	0.7	*3.7*	0.7	*5.9*	0.8	*5.9*
	CNS	0.9	*-0.3*	0.9	*0.5*	1.0	*1.2*	1.0	*2.6*	1.1	*2.0*
	IrE	0.6	*0.3*	0.7	*1.0*	0.8	*2.3*	0.8	*3.7*	0.9	*3.3*
low	whole	0.8	*-0.2*	0.9	*-0.5*	0.9	*0.4*	0.9	*1.1*	0.9	*1.5*
	BNL	0.6	*-0.6*	0.6	*1.0*	0.6	*2.1*	0.7	*4.8*	0.7	*5.3*
	CNS	0.7	*0.9*	0.8	*-1.8*	0.9	*0.2*	0.9	*0.0*	1.0	*-0.2*
	IrE	0.6	*0.2*	0.7	*0.5*	0.8	*1.2*	0.8	*2.8*	0.9	*2.9*
high	whole	0.7	*-0.3*	0.8	*0.7*	0.8	*1.9*	0.9	*3.5*	0.9	*3.3*
	BNL	0.6	*-1.9*	0.6	*4.2*	0.7	*4.8*	0.8	*6.7*	0.9	*6.6*
	CNS	0.9	*-0.5*	0.9	*0.9*	1.0	*1.5*	1.1	*3.0*	1.1	*2.4*
	IrE	0.6	*0.3*	0.7	*1.2*	0.8	*3.0*	0.9	*4.3*	0.9	*3.5*
May 1 - May 14, 1999											
		Forecast lengths									
		00		03		06		09		12	
wind	Region	ref	%	ref	%	ref	%	ref	%	ref	%
all	whole	0.7	*0.0*	0.8	*0.1*	0.9	*0.1*	0.9	*0.3*	0.9	*0.6*
	BNL	0.6	*0.0*	0.7	*0.1*	0.7	*0.5*	0.8	*0.9*	0.8	*1.0*
	CNS	0.8	*0.0*	0.9	*-0.1*	0.9	*0.2*	0.9	*0.5*	0.9	*1.6*
	IrE	0.6	*0.0*	0.7	*0.1*	0.8	*0.4*	0.8	*1.0*	0.9	*1.4*
low	whole	0.8	*0.0*	0.9	*0.0*	0.9	*0.1*	0.9	*0.2*	1.0	*0.3*
	BNL	0.5	*0.0*	0.7	*0.1*	0.8	*0.3*	0.9	*0.8*	0.9	*1.0*
	CNS	0.9	*0.0*	1.0	*0.0*	0.9	*0.1*	0.9	*0.4*	0.9	*0.1*
	IrE	0.6	*0.0*	0.7	*0.1*	0.7	*0.4*	0.8	*0.9*	0.8	*1.4*
high	whole	0.7	*0.0*	0.8	*0.1*	0.8	*0.2*	0.9	*0.5*	0.9	*1.0*
	BNL	0.6	*0.0*	0.7	*0.1*	0.7	*0.6*	0.7	*1.0*	0.7	*1.1*
	CNS	0.8	*0.0*	0.9	*-0.1*	0.9	*0.2*	0.9	*0.5*	1.0	*2.1*
	IrE	0.6	*0.0*	0.7	*0.1*	0.8	*0.3*	0.8	*1.1*	0.9	*1.4*
September 20 - October 4, 1999											
		Forecast lengths									
		00		03		06		09		12	
wind	Region	ref	%	ref	%	ref	%	ref	%	ref	%
all	whole	0.7	*0.0*	0.9	*0.1*	1.0	*0.3*	1.0	*1.1*	1.1	*1.5*
	BNL	0.7	*0.0*	0.8	*0.0*	0.9	*1.2*	0.9	*2.6*	1.0	*3.4*
	CNS	0.7	*0.0*	0.9	*-0.4*	1.0	*-1.3*	1.0	*0.4*	1.1	*0.8*
	IrE	0.6	*0.0*	0.8	*0.0*	0.9	*0.7*	1.0	*1.9*	1.1	*2.5*
low	whole	0.7	*0.0*	0.9	*0.0*	1.0	*0.1*	1.0	*0.6*	1.1	*0.9*
	BNL	0.8	*0.0*	1.0	*-0.8*	1.0	*1.4*	1.1	*2.6*	1.0	*3.6*
	CNS	0.7	*0.0*	0.8	*-0.6*	0.9	*-0.9*	0.9	*-0.9*	1.0	*-1.0*
	IrE	0.5	*0.0*	0.8	*0.1*	0.8	*0.5*	0.9	*1.4*	1.0	*1.9*
high	whole	0.7	*0.0*	0.9	*0.1*	1.0	*0.4*	1.0	*1.4*	1.1	*1.9*
	BNL	0.6	*0.0*	0.8	*0.3*	0.9	*1.1*	0.9	*2.5*	1.0	*3.4*
	CNS	0.8	*0.0*	0.9	*-0.3*	1.0	*-1.3*	1.1	*0.7*	1.1	*1.2*
	IrE	0.6	*0.0*	0.8	*0.0*	0.9	*0.8*	1.0	*2.2*	1.1	*2.9*

Table C.2: RMS and change in RMS (in %) in the difference between forecasted and predicted observed pressure reduced to mean sea level.

2 meter Temperature

June 22 - July 4, 1998

		Forecast lengths									
		00		03		06		09		12	
wind	Region	ref	%	ref	%	ref	%	ref	%	ref	%
all	whole	2.2	*-1.3*	2.1	*-1.1*	2.1	*-1.1*	2.1	*-1.0*	2.1	*-1.0*
	BNL	1.4	*-2.4*	1.5	*0.1*	1.5	*0.3*	1.5	*-0.3*	1.5	*-1.5*
	CNS	1.2	*-2.1*	1.0	*-3.2*	1.0	*-4.1*	1.0	*-7.4*	1.0	*-8.4*
	IrE	1.4	*-1.8*	1.4	*-1.4*	1.5	*-1.8*	1.5	*-2.4*	1.5	*-2.7*
low	whole	2.4	*-0.3*	2.3	*-1.1*	2.2	*-1.2*	2.2	*-0.8*	2.2	*-0.9*
	BNL	1.3	*-1.7*	1.4	*-1.3*	1.4	*-1.8*	1.4	*-2.3*	1.4	*-2.8*
	CNS	1.4	*-1.9*	1.0	*-4.3*	1.0	*-5.2*	1.1	*-9.2*	1.1	*-12.4*
	IrE	1.4	*-0.9*	1.4	*-0.7*	1.5	*-1.4*	1.5	*-1.3*	1.6	*-1.4*
high	whole	1.9	*-2.3*	1.9	*-1.5*	1.9	*-1.3*	1.9	*-1.4*	1.9	*-1.4*
	BNL	1.4	*-2.7*	1.5	*1.0*	1.6	*2.0*	1.6	*1.1*	1.6	*-0.3*
	CNS	1.1	*-2.3*	1.0	*-3.1*	1.0	*-3.9*	1.0	*-7.1*	1.0	*-7.4*
	IrE	1.4	*-2.4*	1.5	*-1.9*	1.5	*-2.1*	1.5	*-3.0*	1.5	*-3.6*

May 1 - May 14, 1999

		Forecast lengths									
		00		03		06		09		12	
wind	Region	ref	%	ref	%	ref	%	ref	%	ref	%
all	whole	2.2	*-1.0*	2.2	*-1.1*	2.2	*-1.0*	2.2	*-1.2*	2.2	*-1.3*
	BNL	1.5	*-1.7*	1.7	*-1.8*	1.7	*-1.6*	1.7	*-2.2*	1.6	*-2.7*
	CNS	1.6	*-0.8*	1.6	*-2.4*	1.5	*-2.0*	1.5	*-1.8*	1.5	*-2.0*
	IrE	1.7	*-4.1*	1.7	*-4.8*	1.7	*-4.8*	1.7	*-5.2*	1.7	*-5.2*
low	whole	2.4	*-0.7*	2.4	*-0.9*	2.4	*-0.9*	2.4	*-0.9*	2.4	*-1.0*
	BNL	1.6	*0.2*	1.7	*-1.1*	1.8	*-0.8*	1.7	*-0.9*	1.7	*-1.1*
	CNS	1.9	*-0.7*	1.9	*-2.4*	1.9	*-3.5*	1.9	*-3.6*	1.9	*-4.2*
	IrE	1.7	*-4.0*	1.7	*-3.7*	1.7	*-3.2*	1.7	*-3.6*	1.7	*-3.6*
high	whole	2.0	*-1.6*	2.0	*-1.2*	2.0	*-1.3*	2.0	*-1.6*	2.0	*-1.6*
	BNL	1.5	*-3.5*	1.6	*-2.3*	1.6	*-2.3*	1.6	*-3.2*	1.6	*-3.9*
	CNS	1.4	*-0.7*	1.4	*-2.4*	1.4	*-1.1*	1.4	*-0.8*	1.4	*-0.9*
	IrE	1.7	*-4.3*	1.6	*-5.7*	1.6	*-6.1*	1.7	*-6.3*	1.7	*-6.4*

September 20 - October 4, 1999

		Forecast lengths									
		00		03		06		09		12	
wind	Region	ref	%	ref	%	ref	%	ref	%	ref	%
all	whole	1.9	*0.1*	1.9	*0.4*	1.9	*0.6*	1.9	*0.8*	1.9	*0.9*
	BNL	1.4	*-0.4*	1.5	*-0.3*	1.5	*0.1*	1.4	*0.8*	1.3	*0.7*
	CNS	1.4	*1.9*	1.4	*3.1*	1.4	*3.8*	1.4	*4.2*	1.4	*4.5*
	IrE	1.4	*0.1*	1.3	*0.5*	1.3	*0.9*	1.3	*1.2*	1.3	*2.2*
low	whole	2.0	*-0.1*	2.1	*0.1*	2.1	*0.2*	2.1	*0.3*	2.1	*0.3*
	BNL	1.4	*-0.3*	1.5	*-0.4*	1.6	*-0.2*	1.6	*0.6*	1.5	*0.1*
	CNS	1.7	*-0.2*	1.7	*0.4*	1.7	*0.2*	1.7	*0.2*	1.7	*1.0*
	IrE	1.4	*-0.2*	1.4	*-0.1*	1.3	*0.0*	1.3	*-0.4*	1.4	*0.4*
high	whole	1.8	*0.3*	1.8	*0.7*	1.8	*1.0*	1.8	*1.4*	1.8	*1.4*
	BNL	1.4	*-0.5*	1.5	*-0.2*	1.4	*0.2*	1.3	*0.9*	1.3	*0.8*
	CNS	1.3	*2.9*	1.3	*4.6*	1.3	*5.5*	1.3	*5.9*	1.4	*6.0*
	IrE	1.4	*0.2*	1.3	*1.0*	1.3	*1.4*	1.3	*2.2*	1.3	*3.3*

Table C.3: RMS and change in RMS (in %) in the difference between forecasted and observed 2 meter temperature.

2 meter Dewpoint Temperature											
June 22 - July 4, 1998											
		Forecast lengths									
		00		03		06		09		12	
wind	Region	ref	%	ref	%	ref	%	ref	%	ref	%
all	whole	2.0	*1.3*	1.9	*1.0*	1.9	*1.2*	1.9	*1.4*	1.9	*1.4*
	BNL	1.3	*3.3*	1.4	*0.0*	1.4	*0.9*	1.4	*2.9*	1.5	*1.8*
	CNS	1.2	*-1.0*	1.2	*-0.3*	1.2	*-0.6*	1.2	*0.4*	1.2	*1.4*
	IrE	1.4	*1.1*	1.4	*1.0*	1.4	*2.3*	1.4	*2.4*	1.4	*4.0*
low	whole	2.1	*1.3*	2.1	*0.4*	2.1	*0.4*	2.1	*0.7*	2.1	*0.2*
	BNL	1.3	*2.5*	1.4	*-0.2*	1.4	*0.9*	1.4	*2.7*	1.4	*2.5*
	CNS	1.3	*-1.7*	1.1	*1.7*	1.1	*0.7*	1.3	*-0.6*	1.3	*0.7*
	IrE	1.4	*2.4*	1.3	*1.6*	1.3	*2.0*	1.3	*1.7*	1.3	*3.1*
high	whole	1.8	*1.4*	1.8	*1.8*	1.7	*2.2*	1.8	*2.5*	1.8	*2.8*
	BNL	1.3	*3.7*	1.4	*0.2*	1.4	*0.8*	1.5	*3.0*	1.6	*1.4*
	CNS	1.2	*-0.8*	1.2	*-0.8*	1.2	*-0.9*	1.2	*0.6*	1.2	*1.7*
	IrE	1.4	*0.5*	1.4	*0.9*	1.4	*2.7*	1.4	*2.8*	1.4	*4.4*
May 1 - May 14, 1999											
		Forecast lengths									
		00		03		06		09		12	
wind	Region	ref	%	ref	%	ref	%	ref	%	ref	%
all	whole	2.1	*0.9*	2.1	*0.2*	2.1	*0.3*	2.1	*0.4*	2.1	*0.3*
	BNL	1.7	*1.1*	1.8	*-1.6*	1.9	*-2.3*	1.9	*-2.5*	1.9	*-3.0*
	CNS	1.4	*0.8*	1.4	*3.1*	1.4	*4.0*	1.4	*5.0*	1.4	*5.5*
	IrE	1.6	*-0.2*	1.5	*-0.5*	1.5	*-0.8*	1.5	*-0.6*	1.5	*-0.4*
low	whole	2.2	*1.5*	2.1	*-0.1*	2.1	*-0.1*	2.2	*-0.2*	2.2	*-0.3*
	BNL	1.7	*1.4*	1.7	*-1.5*	1.7	*-2.0*	1.7	*-2.6*	1.8	*-3.0*
	CNS	1.8	*0.4*	1.7	*1.5*	1.7	*0.9*	1.8	*1.6*	1.8	*1.4*
	IrE	1.6	*0.1*	1.5	*0.3*	1.5	*-0.4*	1.5	*-1.1*	1.5	*-0.9*
high	whole	2.0	*0.2*	2.0	*0.5*	2.0	*0.7*	2.0	*0.9*	2.0	*0.9*
	BNL	1.7	*0.8*	1.9	*-1.7*	2.0	*-2.5*	2.0	*-2.5*	2.0	*-2.9*
	CNS	1.3	*1.1*	1.3	*4.0*	1.3	*5.5*	1.3	*6.7*	1.3	*7.5*
	IrE	1.6	*-0.3*	1.5	*-1.1*	1.5	*-1.0*	1.6	*-0.4*	1.6	*-0.1*
September 20 - October 4, 1999											
		Forecast lengths									
		00		03		06		09		12	
wind	Region	ref	%	ref	%	ref	%	ref	%	ref	%
all	whole	1.9	*0.4*	1.9	*0.5*	2.0	*0.3*	2.0	*0.4*	2.0	*0.5*
	BNL	1.4	*-0.4*	1.4	*-0.1*	1.6	*-0.1*	1.7	*-0.2*	1.7	*-0.3*
	CNS	1.8	*4.0*	1.8	*3.7*	1.8	*3.6*	1.8	*3.4*	1.9	*3.5*
	IrE	1.4	*1.2*	1.4	*1.1*	1.5	*1.3*	1.5	*1.9*	1.5	*2.5*
low	whole	2.0	*-0.1*	2.1	*-0.2*	2.1	*-0.4*	2.2	*-0.4*	2.2	*-0.3*
	BNL	1.5	*-0.2*	1.5	*-0.1*	1.6	*-0.4*	1.8	*-0.1*	1.8	*-0.2*
	CNS	1.6	*2.2*	1.6	*2.2*	1.6	*2.4*	1.6	*1.6*	1.6	*1.1*
	IrE	1.3	*0.3*	1.3	*0.1*	1.4	*0.2*	1.4	*0.4*	1.4	*0.6*
high	whole	1.8	*0.9*	1.8	*1.1*	1.9	*1.0*	1.9	*1.1*	1.9	*1.3*
	BNL	1.3	*-0.5*	1.4	*0.0*	1.6	*0.0*	1.6	*-0.1*	1.7	*-0.2*
	CNS	1.9	*4.4*	1.8	*4.0*	1.9	*3.9*	1.9	*3.7*	1.9	*4.0*
	IrE	1.4	*1.6*	1.4	*1.7*	1.5	*1.8*	1.6	*2.6*	1.6	*3.3*

Table C.4: RMS and change in RMS (in %) in the difference between forecasted and observed 2 meter dew point temperature.

Wind vector difference

June 22 - July 4, 1998

		Forecast lengths									
		00		03		06		09		12	
wind	Region	ref	%	ref	%	ref	%	ref	%	ref	%
all	whole	2.7	-0.3	2.8	-0.4	2.8	-0.3	2.8	-0.1	2.8	-0.1
	BNL	2.2	0.0	2.3	-1.2	2.3	-0.6	2.3	-0.8	2.2	-1.2
	CNS	2.6	0.2	2.7	1.4	2.9	1.6	3.0	0.8	3.0	-0.5
	IrE	2.6	0.0	2.7	-0.7	2.7	-0.6	2.7	-0.6	2.7	-0.4
low	whole	2.1	-0.3	2.3	-0.3	2.3	-0.1	2.2	0.6	2.2	0.6
	BNL	1.6	-0.8	1.8	1.2	1.8	1.2	1.6	3.0	1.6	2.3
	CNS	2.7	1.0	2.8	3.6	3.0	2.1	3.0	1.3	3.1	0.4
	IrE	2.1	0.0	2.4	0.1	2.4	-0.1	2.4	1.1	2.4	0.9
high	whole	3.2	-0.4	3.2	-0.2	3.2	0.0	3.3	-0.2	3.3	-0.3
	BNL	2.6	0.2	2.6	-1.6	2.8	-0.8	2.8	-1.7	2.9	-1.8
	CNS	2.6	0.0	2.7	0.9	2.9	1.5	3.0	0.6	3.0	-0.6
	IrE	2.9	-0.1	2.8	-0.9	2.9	-0.6	2.9	-1.0	2.9	-0.9

May 1 - May 14, 1999

		Forecast lengths									
		00		03		06		09		12	
wind	Region	ref	%	ref	%	ref	%	ref	%	ref	%
all	whole	2.7	-0.1	2.8	0.0	2.8	0.2	2.9	0.2	2.9	0.1
	BNL	2.1	-0.1	2.2	-0.2	2.3	0.8	2.3	0.7	2.3	0.4
	CNS	2.8	-0.2	2.9	0.5	2.9	1.0	3.0	1.4	3.0	1.8
	IrE	2.5	-0.3	2.6	0.0	2.6	0.3	2.7	0.3	2.7	0.1
low	whole	2.0	0.0	2.3	0.4	2.3	0.3	2.3	0.3	2.3	0.3
	BNL	1.6	0.5	1.8	1.9	2.0	1.9	2.0	1.5	2.0	1.0
	CNS	1.9	0.6	2.1	1.2	2.2	0.2	2.1	0.1	2.1	0.1
	IrE	2.0	0.5	2.3	1.0	2.4	1.2	2.3	1.2	2.3	1.2
high	whole	3.3	-0.1	3.3	-0.2	3.3	0.0	3.4	0.1	3.4	0.0
	BNL	2.5	-0.4	2.5	-1.1	2.6	0.2	2.6	0.2	2.6	-0.1
	CNS	3.0	-0.3	3.1	0.4	3.1	1.1	3.2	1.5	3.3	2.1
	IrE	2.9	-0.6	2.8	-0.4	2.8	-0.1	2.9	-0.1	2.9	-0.3

September 20 - October 4, 1999

		Forecast lengths									
		00		03		06		09		12	
wind	Region	ref	%	ref	%	ref	%	ref	%	ref	%
all	whole	3.0	0.0	3.0	-0.1	3.1	-0.2	3.1	-0.1	3.1	-0.1
	BNL	2.6	0.1	2.8	-1.0	2.9	-1.6	2.9	-1.4	2.8	-0.9
	CNS	2.8	0.0	3.0	0.0	3.0	-0.6	3.1	-0.4	3.2	-0.6
	IrE	2.8	-0.1	2.8	-0.3	2.9	-0.5	2.9	-0.2	3.0	-0.4
low	whole	2.4	-0.1	2.5	0.1	2.6	-0.1	2.6	0.0	2.6	-0.1
	BNL	2.2	0.0	2.4	-1.4	2.5	-1.6	2.5	-2.2	2.5	-1.5
	CNS	2.2	0.2	2.4	0.6	2.5	0.5	2.5	1.2	2.6	-1.2
	IrE	2.3	-0.2	2.5	-0.2	2.5	-0.8	2.5	-0.7	2.6	-1.2
high	whole	3.4	0.0	3.5	-0.2	3.5	-0.3	3.6	-0.2	3.6	-0.1
	BNL	2.8	0.1	3.0	-0.6	3.1	-1.6	3.1	-1.3	3.0	-0.7
	CNS	3.0	0.0	3.1	-0.1	3.2	-0.8	3.3	-0.6	3.4	-0.6
	IrE	3.0	-0.1	3.0	-0.3	3.1	-0.4	3.1	0.0	3.2	0.0

Table C.5: RMS and change in RMS (in %) of the wind vector difference between forecasted and observed 10 meter wind.

latent heat flux										
June 22 - July 4, 1998										
	Forecast lengths									
CNS	00		03		06		09		12	
wind	ref	%	ref	%	ref	%	ref	%	ref	%
all	25.9	*12.9*	27.5	*12.9*	26.0	*9.4*	25.5	*7.1*	24.9	*5.8*
low	16.9	*20.6*	14.7	*30.3*	15.3	*25.5*	18.8	*3.5*	17.2	*14.5*
high	27.4	*12.3*	29.3	*12.1*	27.5	*8.5*	26.5	*7.4*	26.1	*5.1*
May 5 - May 14, 1999										
	Forecast lengths									
	00		03		06		09		12	
wind	ref	%	ref	%	ref	%	ref	%	ref	%
all	23.5	*-0.1*	22.3	*-2.1*	22.4	*-3.1*	22.3	*-1.4*	22.6	*1.6*
low	9.2	*4.4*	9.0	*4.9*	9.5	*1.7*	9.7	*1.3*	9.6	*1.0*
high	27.2	*-0.3*	25.8	*-2.5*	25.6	*-3.4*	25.4	*-1.5*	25.6	*1.6*
September 20 - October 4, 1999										
	Forecast lengths									
	00		03		06		09		12	
wind	ref	%	ref	%	ref	%	ref	%	ref	%
all	27.8	*6.5*	30.2	*7.8*	29.4	*7.4*	29.9	*13.1*	30.3	*12.6*
low	14.6	*11.9*	16.7	*17.2*	15.6	*23.1*	15.9	*22.4*	15.0	*17.6*
high	31.4	*6.1*	33.9	*6.9*	33.0	*6.0*	33.5	*12.3*	34.2	*12.3*

Table C.6: RMS and change in RMS (in %) in the difference between forecasted and simulated latent heat flux.

sensible heat flux										
June 22 - July 4, 1998										
	Forecast lengths									
	00		03		06		09		12	
wind	ref	%	ref	%	ref	%	ref	%	ref	%
all	15.3	*8.9*	15.4	*1.6*	15.1	*-2.3*	14.2	*-2.6*	14.4	*-3.3*
low	5.4	*30.0*	4.7	*-2.4*	4.7	*-23.0*	5.2	*-13.6*	4.7	*-7.7*
high	16.6	*8.4*	16.7	*1.7*	16.3	*-2.0*	15.3	*-2.4*	15.5	*-3.2*
May 5 - May 14, 1999										
	Forecast lengths									
	00		03		06		09		12	
wind	ref	%	ref	%	ref	%	ref	%	ref	%
all	16.5	*-4.8*	17.0	*-6.4*	16.6	*-8.0*	16.9	*-4.6*	16.8	*-7.0*
low	5.5	*4.7*	5.1	*4.5*	5.5	*-3.3*	5.0	*-4.2*	4.8	*-4.8*
high	20.4	*0.7*	19.0	*0.9*	18.0	*1.3*	18.1	*2.2*	18.1	*2.3*
September 20 - October 4, 1999										
	Forecast lengths									
	00		03		06		09		12	
wind	ref	%	ref	%	ref	%	ref	%	ref	%
all	16.5	*-4.8*	17.0	*-6.4*	16.6	*-8.0*	16.9	*-4.6*	16.8	*-7.0*
low	8.1	*-4.1*	8.4	*-4.2*	8.2	*-4.8*	7.7	*0.4*	7.8	*-2.8*
high	18.7	*-4.8*	19.2	*-6.6*	18.7	*-8.2*	19.1	*-4.9*	19.0	*-7.2*

Table C.7: RMS and change in RMS (in %) in the difference between forecasted and simulated sensible heat flux.

Appendix D

Validation study of AVHRR SST's in framework of Rest3D project

Summary report of study carried out by KNMI in framework of BCRS-project Rest3D (2.1/AP-04)

D.1 Introduction

The Rest3D project is carried out by WL/Delft Hydraulics with participation of KNMI and RIKZ/Rijkswaterstaat. The aim of the project was to research the use of satellite measured SST's in a numerical 3D water temperature model of the North Sea. For this purpose the AVHRR SST product of KNMI was used as input for the project. The task of KNMI in Rest3D was to validate the methodology used in the production of weekly SST composites. The accuracy with which Sea Surface Temperature (SST) can be measured using satellite infrared (IR) radiometers is limited primarily by uncertainties in the correction for atmospheric effects upon the measured radiance. This chapter reports the results of a study in which two different atmospheric correction algorithms of NOAA-AVHRR IR data are validated and intercompared using high quality in-situ measured SST's. One algo-

rithm, developed by the Rutherford Appleton Laboratory (RAL) in the UK, is applied operationally at KNMI for the last 10 years. The other algorithm is operationally applied by NOAA to produce SST maps of the North Atlantic Ocean which are used by many users in the USA and Europe. The two "split-window" IR channels of the AVHRR are chosen so that atmospheric effects are different for each channel. By using a linear combination of the two channels an atmospherically corrected SST can be derived without the additional need for actual information on the state of the atmosphere:

$$SST = A_0(\alpha) + A_1(\alpha) * T_4 + A2(\alpha) * T_5 \tag{D.1}$$

T_4 and T_5 are the brightness temperatures measured in channel 4 and 5; A_0, A_1 and A_2 represent empirically determined coefficients and are airmass (α) dependent. The determination of the coefficients is a one-time effort. Once a suitable set of coefficients is determined it can be applied in numerous situations. The RAL coefficient set is determined in the early 80's using NOAA-7 data valid for both day- and nighttime images and has not been updated ever since for other NOAA-satellites. NOAA uses its own split-window coefficient set (called MCSST) for the production of operational global SST data sets that are applied world wide in many oceanic and meteorological environments. Contrary to the RAL coefficient set NOAA determined different coefficient sets for each different NOAA satellite and for day and night images.

D.2 Objective of study

Since the RAL algorithm is developed using NOAA-7 data and KNMI applies the same coefficient sets ever since for the successive NOAA satellites (8 until 15) the main objective of this study was to verify the accuracy of the RAL algorithm if applied to successive satellites and also to compare the RAL SST's with NOAA/NESDIS SST's. The findings set up-to-date error bars to the NOAA-AVHRR data sets as used in the Rest3D study of WL/Delft Hydraulics and also possible result into recommendations for adjustments of the procedures used in the operational SST production system at KNMI.

D.3 Working method

To coincide this work in the other parts of the Rest3D project it was chosen to use NOAA-AVHRR image data of 1994 for the validation work. In order to calculate MCSST's (using the NOAA/NESDIS coefficients) raw AVHRR image data were needed. These are not archived at KNMI. Therefore, raw AVHRR images of the North Sea had to be ordered from AVHRR archives in Europe (Dundee Satellite Station in the UK and DLR/DFD in Germany). 31 passes were selected and ordered. Selection was based on a combination of cloud free situations and the availability of as much as possible collocated in-situ measurements. For this purpose in-situ measured SST's from Rijkswaterstaat were available (the routine MS "Holland" cruises along the Dutch coast). In 1994 the NOAA-11 (night and afternoon passes) and the NOAA-12 (morning and evening passes) were operational. The raw image data was processed twice: once using the RAL algorithm as implemented in the operational production system at KNMI and once using the NOAA/NESDIS MCSST algorithm (both algorithms are described in chapter 2). Each SST image is navigated very carefully to enable an accurate collocation of the in-situ SST measurements and the SST pixel values in the image. By regression analysis the mean bias (in-situ minus AVHRR), the RMS and the standard deviation of all samples of cloud free AVHRR SST-pixel values and collocated in-situ SST's were calculated. This was done for both AVHRR SST's and for each NOAA pass. In order to evaluate the composite procedure also composite images are produced (composed of the single pass images) and validated using the same in-situ data. Also the operational weekly AVHRR SST composites as used by WL/Delft Hydraulics are validated simultaneously (MCSST weekly composites off course were not available for this study).

D.4 Results

In Table D.1 the statistics of the single pass images are summarised in different classes with the aim to enable an objective analysis of the performance of the two SST-algorithms. The same is done in table 2 but now the statistics of the SST composite validation are summarised.

In this study it was tried to evaluate the accuracy of satellite measured SST's

Selection	SST-Algorithm	Bias	RMS	Standard Deviation	Number of samples
All images	RAL	-0.01	0.60	0.44	405
	MCSST	-0.35	0.71	0.47	
NOAA 11 (day)	RAL	-0.17	0.64	0.54	158
	MCSST	-0.62	0.91	0.58	
NOAA 11 (night)	RAL	-0.07	0.51	0.31	65
	MCSST	-0.32	0.66	0.35	
NOAA 12 (evening)	RAL	0.34	0.41	0.23	14
	MCSST	0.01	0.29	0.25	
NOAA 12 (morning)	RAL	0.12	0.50	0.41	168
	MCSST	-0.16	0.58	0.43	
Sun angle $< 20^o$	RAL	0.19	0.53	0.32	204
	MCSST	-0.14	0.56	0.36	
Sun angle $> 20^o$	RAL	-0.21	0.67	0.56	201
	MCSST	-0.49	0.86	0.58	
Exact time collocated samples (< 1 hour)	RAL	0.18	0.45	0.41	24
	MCSST	-0.14	0.45	0.43	

Table D.1: Summarised statistics of validation of single pass SST images in 1994

Type of composite	No. of images in compos.	SST-Algorithm	Bias	RMS	Standard Deviation	Number of samples
Rest3D selected images	3 - 5	RAL	-0.57	0.90	0.58	130
		MCSST	-1.04	1.24	0.63	
Oper. weekly KNMI comp. (all images)	± 40	RAL	-0.82	1.09	0.64	130
Oper. weekly KNMI comp. (only nighttime images)	± 20	RAL	-0.21	0.60	0.48	127

Table D.2: Summarised statistics of validation of composite SST images in 1994

by comparison with in-situ measured SST's. The in-situ data set used is comprised of very accurate ship measurements of the temperature just below the water surface. Still discrepancies between these ship measured SST's and the satellite SST's may occur without one of the two being inaccurate. Several factors that contribute to these discrepancies can be identified: cloud contamination of pixels, uncertainties in collocation of in-situ and satellite measurements, difference in observation time between in-situ and satellite SST's, strong near-surface vertical temperature gradients, caused by the di-

urnal course of air-sea heat exchange at the sea surface. The last factor can be extreme under conditions of high insolation (midday in the summer) and low surface wind speed. In these cases the local skin temperature (as measured by the satellite) can be heated several degrees within a few hours (so called "hot spots" in an AVHRR image).

All these factors are not disturbing an objective intercomparison of the RAL and MCSST algorithms. Validation statistics of both algorithms are derived under the same conditions and by using the same in-situ data sets. The summarised statistics in table 1 show that in most cases the RAL algorithm (as used operational at KNMI) provides more accurate SST's than the MCSST algorithm of NOAA/NESDIS. The mean bias (in-situ minus AVHRR) of the RAL SST's is almost zero while the MCSST algorithm overestimates the SST by 0.35^{o}C. Also the RMS of the RAL algorithm is a bit lower. The overestimation of the SST by the MCSST algorithm becomes even more obvious during daytimes in the summer (up to a degree overestimation). Part of the overestimation is real due to the vertical temperature gradient under these conditions. Still, in most cases the MCSST overestimation is much stronger than the overestimation by the RAL algorithm under these "hotspot" conditions.

In general the statistics found in this validation study are in good agreement with validation results for the MCSST algorithm found in the literature [Anderson, et al.]: bias: 0.20 and stand. dev.: 0.7. Comparing these statistics with the RAL statistics (bias: 0.01 and stand. dev.: 0.44) it can be concluded that the application of the RAL algorithm for the calculation of SST images of the North Sea is most preferred. The higher accuracy provided by the RAL algorithm is confirmed by the validation of the composites of Rest3D selected single pass images (see Table D.2). The mean bias of the RAL SST's is about 0.5 degree better (closer to zero) than the MCSST SST's. Both biases indicate an overestimation of the SST. This is due to the fact that the composites are derived by picking for each pixel the maximum SST in the row of single pass images. Therefore, hot spots, occurring in daytime images, are included in the composite images. KNMI has recognised this problem before and therefore produces in the summer months also weekly SST composites made of only nighttime and early morning images. Now the daytime heated SST's are not included in the composite. It can be concluded from the statistics in table 2 that the problem of overestimated

SST's is nearly solved by using this "nighttime" composite. Also the RMS and standard deviations of the nighttime composites are much lower than those of the "all image" composites.

D.5 Conclusions

This study has shown that the RAL algorithm used at KNMI for more than 10 years now still is the best possible option to derive accurate AVHRR SST images on an operational basis. The satellite and time-of-the-day independent RAL algorithm provides better results than the NOAA/NESDIS MCSST algorithm, which is adjusted for each different satellite and period of the day.

The accuracy of AVHRR SST imagery of the North Sea as produced at KNMI can believed to be around 0.5^{o}C. Nighttime images contain in most cases slightly too low SST values and daytime images slightly too high (especially in summer times).

The procedure for the production of composite SST images of the North Sea is proven to be quite optimal. The timeliness of the SST values in the composites can be improved by updating the weekly composites every day instead of once a week.

The National Remote Sensing Programme 1990-2000, (NRSP-2) is implemented under the responsibility of the Netherlands Remote Sensing Board (BCRS) and coordinated by the Ministry of Transport and Public Works.

The objectives of the NRSP-2 are: to secure the long-term integration of the operationel use of remote sensing through temporary stimulation in the user-sectors of government and industry, to strengthen the development of remote sensing applications and the expansion of the national infrastructure.

Publication of:

Netherlands Remote Sensing Board (BCRS)
Programme Bureau
Rijkswaterstaat Survey Department

P.O. Box 5023
2600 GA Delft
The Netherlands
Tel.: +31 (15) 269 11 11
Fax: +31 (15) 261 89 62
E-mail: p.b.bcrs@mdi.rws.minvenw.nl
BCRS homepage: http://www.minvenw.nl/rws/mdi/bcrs